Size distributions and mixtures of dust and black carbon aerosol in Asian outflow: Physiochemistry and optical properties

A. D. Clarke,[1] Y. Shinozuka,[1] V. N. Kapustin,[1] S. Howell,[1] B. Huebert,[1] S. Doherty,[2] T. Anderson,[2] D. Covert,[2] J. Anderson,[3] X. Hua,[3] K. G. Moore II,[1] C. McNaughton,[1] G. Carmichael,[4] and R. Weber[5]

Received 24 November 2003; revised 4 March 2004; accepted 18 March 2004; published 8 June 2004.

[1] During Transport and Chemical Evolution over the Pacific (TRACE-P) and Asian Aerosol Characterization Experiment (ACE-Asia) we measured the dry size distribution of Asian aerosols, their state of mixing, and the optical properties of dust, black carbon (BC) and other aerosol constituents in combustion and/or dust plumes. Optical particle sizing in association with thermal heating extracted volatile components and resolved sizes for dust and refractory soot that usually dominated light absorption. BC was internally mixed with volatile aerosol in ~85% of accumulation mode particles and constituted ~5–15% of their mass. These optically effective sizes constrained the soot and dust size distributions and the imaginary part of the dust refractive index, k, to 0.0006 ± 0.0001. This implies a single-scatter albedo, ϖ (550 nm), for dust ranging from 0.99+ for $D_p < 1$ μm to ~0.90 at $D_p = 10$ μm and a size-integrated campaign average near 0.97 ± 0.01. The typical mass scattering efficiency for the dust was ~0.3 $m^2\ g^{-1}$, and the mass absorption efficiency (MAE) was 0.009 $m^2\ g^{-1}$. Less dust south of 25°N and stronger biomass burning signatures resulted in lower values for ϖ of ~0.82 in plumes aloft. Chemically inferred elemental carbon was moderately correlated with BC light absorption ($R^2 = 0.40$), while refractory soot volume between 0.1 and 0.5 μm was highly correlated ($R^2 = 0.79$) with absorption. However, both approaches yield an MAE for BC mixtures of ~7 ± 2 $m^2\ g^{-1}$ and higher than calculated MAE values for BC of 5 $m^2\ g^{-1}$. The increase in the mass fraction of soot and BC in pollution aerosol in the presence of elevated dust appears to be due to uptake of the volatile components onto the coarse dust. This predictably lowered ϖ for the accumulation mode from 0.84 in typical pollution to ~0.74 in high-dust events. A chemical transport model revealed good agreement between model and observed BC absorption for most of SE Asia and in biomass plumes but underestimated BC for combustion sources north of 25°N by a factor of ~3. *INDEX TERMS:* 0305 Atmospheric Composition and Structure: Aerosols and particles (0345, 4801); 0350 Atmospheric Composition and Structure: Pressure, density, and temperature; 0360 Atmospheric Composition and Structure: Transmission and scattering of radiation; 0365 Atmospheric Composition and Structure: Troposphere—composition and chemistry; 0368 Atmospheric Composition and Structure: Troposphere—constituent transport and chemistry; *KEYWORDS:* dust, black carbon, absorption, single scatter albedo

Citation: Clarke, A. D., et al. (2004), Size distributions and mixtures of dust and black carbon aerosol in Asian outflow: Physiochemistry and optical properties, *J. Geophys. Res.*, *109*, D15S09, doi:10.1029/2003JD004378.

1. Introduction

[2] The radiative properties of atmospheric aerosol depend upon the size and nature of the mixing of these absorbers with other common atmospheric aerosol such as sulfates, ammonium, nitrates, organic carbon, and water. These mixtures range between internal (multiple components within a particle) and external (different components in different particles). Because many of the components are hygroscopic and take up water as a function of relative humidity (RH), the nature of the soluble and insoluble components of the mixtures determines the size, refractive index, and optical properties under ambient RH conditions. Hence efforts that include the modeling of aerosol radiative

[1]School of Ocean and Earth Science and Technology, University of Hawaii at Manoa, Honolulu, Hawaii, USA.
[2]Department of Atmospheric Sciences, University of Washington, Seattle, Washington, USA.
[3]Environmental Fluid Dynamics Program, Arizona State University, Tempe, Arizona, USA.
[4]Department of Chemical and Biochemical Engineering, University of Iowa, Iowa City, Iowa, USA.
[5]School of the Earth and Atmospheric Sciences, Georgia Institute of Technology, Atlanta, Georgia, USA.

0148-0227/04/2003JD004378$09.00

properties or the retrieval of aerosol properties from remote sensing and optical measurements need to properly account for these size-dependent properties.

[3] It is well known that the light-absorbing black carbon (BC) mass is generally found in the submicrometer sizes, while most dust mass is in supermicrometer sizes. BC has a strong light absorption per unit mass (or mass absorption efficiency, MAE) and submicrometer refractory dust has much lower MAE. The complex refractive indices of ambient atmospheric soot, BC, and dust are essential parameters for modeling their light absorption, but they remain poorly characterized. Soot can be a complex mix of components that include absorbing BC. The influence of size, morphology, aggregation, composition, refractive index, and other characteristics on BC optical properties is carefully examined by *Fuller et al.* [1999] (hereinafter referred to as FMK).

[4] Dust optical properties are uncertain for different reasons. In the aerosol phase the particles have irregular shapes difficult to model [*Kalashnikova and Sokolik*, 2002; *Mishchenko et al.*, 1997] and may have weathered surfaces that differ chemically from the parent material or may be coated with other nonabsorbing or absorbing components. *Sokolik and Toon* [1999] have revised earlier estimates of dust complex refractive index downward and suggest a k value for dust with 1% hematite lies somewhere near 0.001 at a wavelength of 0.55 μm. *Kalashnikova and Sokolik* [2002] use this value in their model and report a range of single-scatter albedo between 0.969 and 0.978 depending on the dust shape for an assumed lognormal distribution with a number median diameter of 1 μm. These recent simulated values for single-scatter albedo are in good agreement with in situ observations [*Anderson et al.*, 2003; *Clarke and Charlson*, 1985; *Clarke et al.*, 2001; *Kaufman et al.*, 2001] and the observations discussed here.

[5] In this paper we focus attention upon the measured size-resolved light-absorbing properties of dust and BC. These are discussed in conjunction with characteristics of the accumulation and coarse mode aerosol, the soot component of the aerosol, and the concurrent elemental carbon (EC) measurements. Hence it is important to clarify these terms in this paper. BC is used here as the light-absorbing component of the soot aerosol. We use the word "soot" here to represent the combination of BC with other species emitted near the combustion source that might be mixed with it such as organic carbon (OC) or pyrolized and unburned fuel, etc. At times, "soot/BC" is used to emphasize this link. In this study, fly ash is considered separate from soot since it is generally observed as particles with a distinct and separate morphology [*Shi et al.*, 2003]. Because most of our samples were hours to days away from the combustion source, this evaluation reflects aged soot emissions often associated with other species that largely compose what we refer to as the submicrometer accumulation mode. The term EC is retained for the operationally defined carbon mass concentration inferred from the evolution of CO_2 detected upon sample filter heating in O_2 [*Huebert et al.*, 2003].

[6] During the spring of 2001 we participated in two aircraft experiments as part of Asian Aerosol Characterization Experiment (ACE-Asia) [*Huebert et al.*, 2003] and NASA Transport and Chemical Evolution over the Pacific (TRACE-P) [*Jacob et al.*, 2003] studying the microphysical and optical properties of Asian aerosol advected over the North Pacific. These sequential experiments with similar aerosol instrumentation provided a unique opportunity to investigate outflow from east Asia between 5°N and 50°N during the same season. The TRACE-P experiment (24 February to 10 April 2001) was initially based in Hong Kong and after 17 March was based in Yakota, Japan. ACE-Asia flights were based out of Iwakuni, Japan, from 31 March to 4 May 2001. Most ACE-Asia measurements were made using the low-turbulence inlet and the TRACE-P measurements employed our shrouded solid-diffuser inlet, both of which were evaluated in the PELTI experiment (B. Huebert et al., Measurements of organic and elemental carbon in Asian outflow during ACE-Asia from the NSF/NCAR C-130, submitted to *Journal of Geophysical Research*, 2004, hereinafter referred to as Huebert et al., submitted manuscript, 2004). The last two TRACE-P flights were flown in conjunction with the first two ACE-Asia flights allowing us to quantitatively compare instrumentation on both aircraft [*Moore et al.*, 2004]. Differences were small and do not affect the analysis or conclusions in this paper.

2. Instrumentation

[7] The aircraft aerosol data discussed here include measurements of number, size, composition, and optical properties along with related measurements of gas phase species. These include the following:

[8] 1. Aerosol size distributions were obtained from a laser optical particle counter (OPC, a modified LAS-X, Particle Measurement Systems, Boulder, Colorado). Optically effective size (OES) distributions were obtained between diameters of 0.1 and ~10 μm based on spherical calibration particles with a refractive index of 1.588 up to 2 μm and 1.54 above that. Because these OES distributions include effects of shape, they are most useful for modeling optical properties. Adjustments to aerodynamic or geometric sizes require additional information on shape, density, and refractive index. We use the subscript OE to identify parameters based on OES measurements such as diameter, D_{OE}.

[9] 2. The OPC was operated with thermo-optic aerosol discriminator in order to infer size-dependent volatility by cycling aerosol through heaters at 150°C and at 300°C (ACE-Asia) or 350°C (TRACE-P). Heating to 150°C is designed to drive off low-temperature volatiles (sulfuric acid and some nitrates and OC), while heating to 300°C+ is designed to volatilize ammonium sulfate [*Clarke*, 1991]. The residual "refractory" aerosol includes most light-absorbing soot (and black carbon, BC) below ~1 μm, while the larger refractory component is generally dust or occasionally sea salt.

[10] 3. A radial differential mobility analyzer (DMA) provided additional size information between 0.007 and 0.15 μm. Dual DMAs were also operated periodically in tandem DMA mode (TDMA) with similar thermal analysis, although heating to 350°C was often employed. One DMA selects a specific size for thermal conditioning before scanning with a second DMA. DMA samples were collected over 20 s and held in a lagged aerosol grab chamber [*Clarke et al.*, 1998] for subsequent DMA analysis.

[11] 4. Total aerosol number concentrations were measured at 1 Hz with an ultrafine condensation nuclei (CN) counter (TSI 3025) and with two CN counters (TSI 3760 or TSI 3010) both operated at 40°C and 360°C. CN counters operating at 300°C+ reveal the refractory number concentration of the aerosol that often provides a rapid indication of air mass character not always evident in the total concentration [*Clarke et al.*, 1997].

[12] 5. Two three-wavelength TSI 3563 nephelometers were used on the C-130 during ACE-Asia to simultaneously measure coarse and fine aerosol light scattering. The latter was measured using a 1 μm aerodynamic impactor [*Anderson et al.*, 2003]. TRACE-P employed a similar TSI nephelometer but with an identical impactor cycled sequentially to alternately measure total and submicrometer light scattering.

[13] 6. Light absorption was measured with a particle soot absorption photometer (PSAP, Radiance Research) on both aircraft with and without a 1 μm aerodynamic impactor. Again, total and submicrometer measurements were continuous on the C-130 and measured alternately on the P3-B. Corrections for artifact absorption due to scattering were applied after *Bond et al.* [1999]. In conjunction with the light scattering, this also established coarse and fine aerosol single-scatter albedo [*Anderson et al.*, 2003]. On TRACE the PSAP operated at ~4–5 L min^{-1} resulting in impaction losses of ~50% for 4 μm particles, while on ACE it was operated at 1 L min^{-1}. Our postexperiment tests found this to result in impaction losses of 50% at 12.5 μm. The higher flow rate made coarse particle losses potentially greater on TRACE, but this effect was seldom significant because few dust events were encountered [*Bond et al.*, 1999]. Because OPC sizes were not well resolved above ~10 μm, this means that both PSAP and OPC characterized similar size distributions such that they can be effectively compared.

[14] 7. A particle into liquid sample (PILS) [*Orsini et al.*, 2003; *Weber et al.*, 2001] employs a steam saturator followed by impaction of wet aerosol for collection and measurement of major ions every few minutes using ion chromatography. The PILS provides soluble (e.g., sulfate, nitrate) species that influence refractive index and hygroscopic behavior up to diameters near 1.3 μm with ~4 min resolution.

[15] 8. Elemental carbon (EC) and organic carbon (OC) are operationally defined measures of nominally light-absorbing carbon and organic carbon based on the thermal evolution of CO_2 and were measured on samples collected from the ACE-Asia aircraft and analyzed using the Sunset Labs instrument [*Huebert et al.*, 2003, also submitted manuscript, 2004] with an average uncertainty of 30% for these data. This instrument sampled off a separate solid diffuser inlet.

[16] Heating of the aerosol (RH < 40%) prior to analysis by both the DMA and OPC was an important feature of our measurements on both experiments. Primary emissions of refractory particles are often present in both fine (soot, fly ash) and coarse sizes (sea salt, dust) and are thermally separable from most volatile sulfates, nitrates, and OC. In remote oceanic regions we have previously shown how aerosol volatility can be linked to the volatile sulfate aerosol and its relative neutralization by ammonia [*Clarke*, 1991]. In spite of the greater complexity of the Asian aerosol chemistry we have been able to quantitatively relate our observed volatile volume to soluble ions obtained from the PILS technique between diameters of 0.1 and 1.2 μm. These sizes contain most of the volatile mass and the soluble mass. This study yielded a regression leg average OPC and PILS mass with a slope of 1.05 and an R^2 of 0.78 and supports our use of volatility as an indicator for aerosol chemistry. The details of this comparison are the subject of a separate paper that focuses upon the humidity response of the Asian aerosol (S. G. Howell, personal correspondence, 2004).

3. TRACE-P and ACE-Asia Experiments

[17] Comparison of data sets from different experiments can often be problematic due to different instrumentation or sampling approaches. Consequently, deliberate side-by-side flights were made for the TRACE-P P3B and the ACE-Asia C-130 during the few days these two experiments overlapped. In spite of differences in inlet types, aerosol sizing and optical properties agreed within instrument uncertainty at all altitudes [*Moore et al.*, 2004] and provide confidence that these and the related optical measurements discussed here are comparable and can be combined.

[18] Figure 1 shows mission-average vertical profiles for scattering, absorption, and single-scatter albedo for both experiments. Aerosol absorption is present throughout both study regions in the lowest 3 km, but concentrations vary with sources from regional scales, urban center scales, and down to plume scales of several kilometers. TRACE-P flight data have been separated into data collected south and north of 25°N in view of chemical and meteorological differences evident for these regions [*Jacob et al.*, 2003]. The 19 ACE-Asia flights were north of 25°N (Figure 1, bottom) and are compared to the five TRACE-P flights north of 25°N (Figure 1, top) even though the number of flights, time periods and meteorological conditions differed. The average TRACE-P data south of 25°N (Figure 1, middle) suggest a dominant scattering and absorbing layer below 1 km with a thicker 1-4 km layer above. The latter was characterized by moderate scattering and high absorption but with transitions to lower and more typical values for both above 4 km. This layer aloft also has chemical signatures associated with biomass burning [*Ma et al.*, 2004]. The associated profile for ϖ shows highest values near 0.92 at the surface that drop to ~0.8 near 2 km. Variation in ϖ around this value continues up to 6 km altitude.

[19] The data north of 25°N from both TRACE-P (Figure 1, top) and ACE-Asia (Figure 1, bottom) reveal similar vertical profiles that differ from the data south of 25°N. High scattering and absorption values below 1 km trend to lower values aloft. North of 25°N, ϖ has values near 0.92 at the surface but increases with altitude to values near 0.95 at 6 km. As discussed below, this increase is largely due to the presence of dust aerosol [*Anderson et al.*, 2003], and the greater frequency of the dust events during ACE-Asia contributes to the higher and more stable average scattering and absorption aloft for these data. Note that average near-surface properties for all three examples are similar and show ϖ near 0.925 ± 0.015 (circled) in contrast to the variability evident aloft. These surface values provide

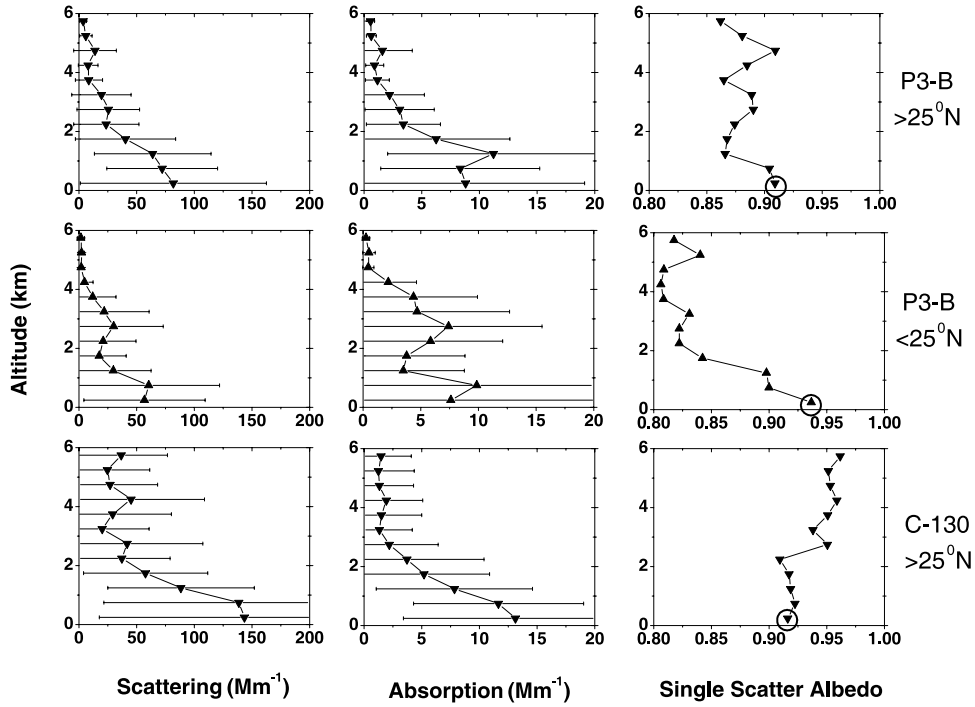

Figure 1. Average vertical profiles of aerosol light scattering, light absorption, and ϖ for TRACE-P north and south of 25°N and for ACE-Asia north of 25°N. Data have been binned over 500 m altitude ranges and shown with 1 standard deviation as measure of variability except for the resulting derived values of ϖ. High relative absorption aloft south of 25°N is related to biomass sources that result in low ϖ, while higher dust scattering in ACE-Asia aloft yields higher ϖ values. Note that surface values of ϖ (circled) are similar at all locations and do not reflect the differences in column values.

a poor representation of the column properties in both regions and emphasize the importance of aircraft data in establishing aerosol and optical properties over the atmospheric column. The indicated standard deviation for this average profile reveals the large variability in the aerosol. These variations below the inversion were often on the order of tens of percent over vertical scales of 100 m or less and horizontally over scales of a few kilometers.

3.1. Observed Morphology of Dust and Soot

[20] It is important to keep in mind the physical properties of the aerosol when considering its optical effects. Figure 2 illustrates actual scanning electron micrographs of aerosol types sampled during flight 13 of ACE-Asia over the Yellow Sea at altitudes of 5500, 700, and 250 m. The high-altitude sample shows generally sharp-edged dust aerosol with some occasional soot particles, but the size of soot clusters, their abundance, and their attachment to dust surfaces increase at low altitudes. Most isolated soot clusters and solitary carbon spheres (carbon cenospheres) have a graphitic nature (open circles) and may have been originally coated with volatiles. Other features are identified in Figure 2. Note that the high vacuum combined with thermal heating of the particles by the high beam current during this analysis drives off many volatile species such as sulfate and low-temperature OC [*Li et al.*, 2003] leaving the more refractory components shown here. We presume that the dust and soot particles remaining in these images are similar to those detected in the 300°C OPC OES distributions. The complexity of these mixtures and shapes raises serious questions regarding what is meant by the size of the aerosol since diameters that represent the actual geometric, aerodynamic, optical, and effective mass of these particles are likely to be quite different. Hence we emphasize here the value of optically effective sizes in the interpretation and calculation of aerosol optical properties.

3.2. Size Distributions and Volatility

[21] As mentioned earlier, we discuss here the optically effective sizes based on scattering properties detected by the OPC. These are most useful for regeneration of optical properties via Mie scattering, but physical sizes may be quite different. Variability in aerosol optical properties are also related to size-dependent variations in composition that are also linked to aerosol volatility. Several examples of OPC thermally resolved OES distribution data from flight 13 of ACE-Asia are shown in Figure 3 for diameters between 0.1 and 10 μm. Here we assumed the coarse particle enhancement in the LTI was largely compensated by similar losses in the sample line (Huebert et al., submitted manuscript, 2004). This size range generally encompasses most aerosol masses that influence aerosol radiative effects at visible wavelengths. Each case is an average of several distributions accumulated under similar conditions so that volatility is well characterized and not a result of concentration variations over a single 90 s measurement period. Data are presented both in a logarithmic format to expose the full range of concentrations and as

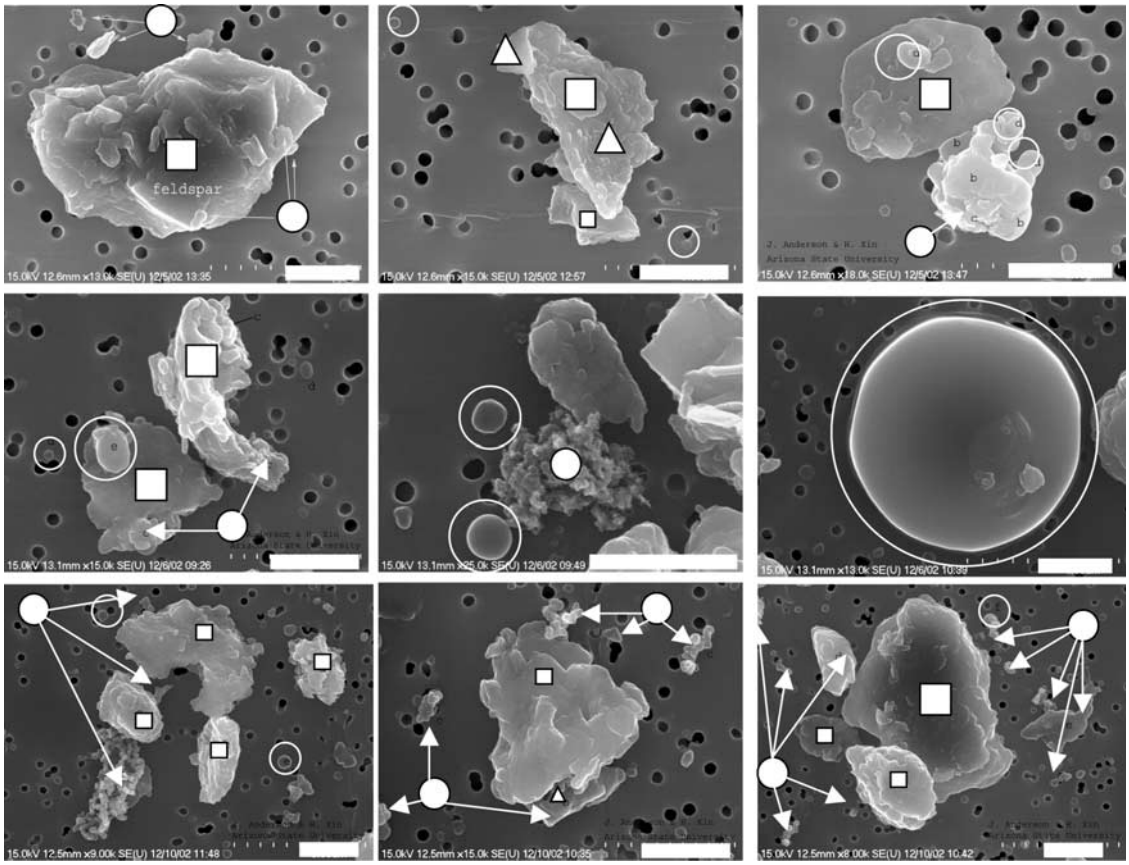

Figure 2. Scanning electron micrograph images for three flight altitudes (5500 m (Figure 2, top); 700 m (Figure 2, middle); 250 m (Figure 2, bottom)) on flight 13 discussed at various places throughout text. White bars at bottom of each plot are 2 μm long. Some particles identified by emission spectra are labeled for reference. Square, various forms of aluminosilicates; triangle, calcium carbonate; open circle, large spherical graphitic carbon (carbon cenosphere); solid circle, more typical soot carbon aggregates. All small, unlabeled spherical particles are also graphitic soot (BC). Any originally associated volatile material has been vaporized by the high electron beam intensity. Note the large carbon cenosphere in Figure 2 (middle right) that is at low concentrations but more prevalent in this region than many others and the large aggregated BC cluster in Figure 2 (middle middle). Submicrometer fly ash as silicate cenospheres are also often seen but not in these images. Soot particles are present at all altitudes and seen attached to dust but relative concentrations of soot increase significantly at lowest altitudes. (See text for details.)

linear volume distributions (where the area under each curve is proportional to volume) in order to better reveal relative contributions.

[22] This flight was selected because it included very high dust concentrations mixed with a range of soot concentrations. Figure 3 (top) illustrates a moderate dust event associated with low measured submicrometer light absorption and little volatility between 150°C and 300°C between 0.1 and 0.5 μm. Some nitrates or volatile OC can possibly contribute to components volatile at 300°C, but sulfate is a major constituent [*Weber et al.*, 2003]. The refractory dust is shown as a linear volume distribution (area under plot proportional to volume) in Figure 3 (top), corresponding to ~125 μg m^{-3}, but the volatile component is no longer resolved for this mode.

[23] Figure 3 (middle) illustrates a higher dust concentration on the order of 1000 μg m^{-3} mixed with more pollution aerosol, and the volatile accumulation mode volume corresponds to ~5 μg m^{-3}. This and the refractory (300°C) component are an order of magnitude larger than the upper row, but this is not evident on the linear plot due to the high-dust concentration. Note that the peak diameter for dust volume shifts to larger sizes for the highest dust case (Figure 3, middle). Figure 3 (bottom) is a low-dust case associated with a moderate submicrometer light absorption coefficient and moderate volatile component (typical of most TRACE-P data). The amount of volatile accumulation mode corresponds to a mass of ~20 μg m^{-3} (~4 times the previous case), while the coarse particle dust is only ~50 μg m^{-3} (<5% of the previous case). Both modes are well resolved on the linear volume plot (Figure 3, right). The heated size distributions reveal most volatility is present for sizes below ~0.6 μm, but unlike the previous two cases, a significant fraction of the coarse mode volume below ~2 μm is evident as volatile coatings on the coarse dust aerosol. The apparent differences in volatility for the larger

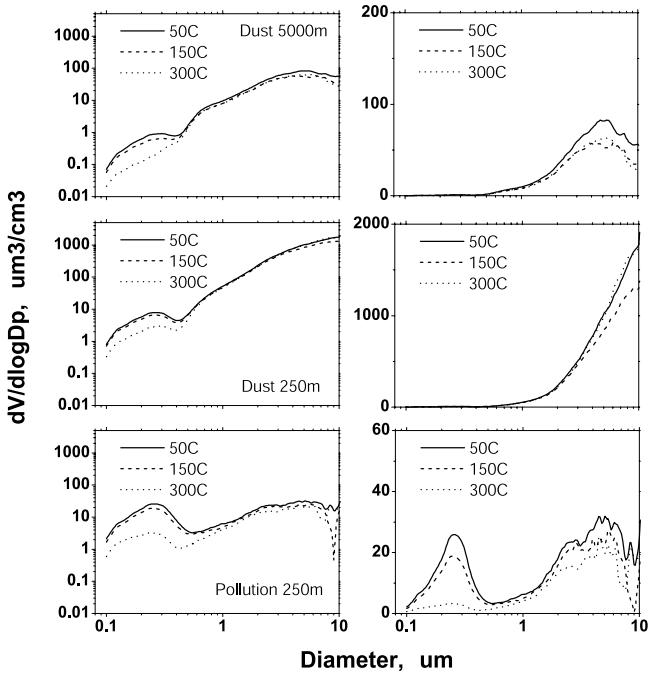

Figure 3. Examples of OPC optically effective size (OES) distributions showing application of thermal analysis in both logarithmic and linear formats for $dV/d(\log D_p)$ for three environments with different dust concentrations on ACE-Asia flight 13. (top) Moderate dust with very low soot/BC in accumulation mode, (middle) very high dust with moderate-low soot/BC in accumulation mode at 250 m, and (bottom) low dust with high soot/BC in accumulation mode and large volatile component at 250 m (see text).

sizes are not statistically significant because of low count statistics. Note that Figure 3 (bottom left) shows that the refractory mode present between 0.1 and 0.6 μm is much more pronounced than for the very high-dust case and the volume peak on the linear scale stands out clearly relative to the dust. This demonstrates that the submicrometer refractory mode is related to the accumulation mode pollution component and not the dust distribution.

3.3. State of Mixing in the Accumulation Mode and Smaller Sizes

[24] The refractory soot and dust discussed above are the primary absorbing aerosol. However, the volatile species have a large influence on the scattering and the state of mixing of the aerosol (internal or external) and are important for proper understanding of overall aerosol optical effects. Mixing state can often be inferred from size-resolved volatility. If mass changes upon heating but the integral number does not, then the volatile component must be internally mixed with the refractory component. If both number and mass change, then some or all particles may be externally mixed, depending upon the change in the size distribution. Hence we use measurements from both the OPC (Figure 3) and DMA to resolve changes upon heating for both volume and number over the size ranges of interest.

[25] Although most aerosol volume and optical properties present in diameters above 0.1 μm are resolved by the OPC, the ambient number distribution generally contains many particles smaller than this diameter. In order to better understand what controls the total particle number it is valuable to resolve the complete size distributions of both total and refractory aerosol. Hence we have extended our volatility techniques down to 0.01 μm diameter through use of our DMA and Tandem DMA (TDMA) instrumentation. Figure 4 shows examples of DMA, TDMA, and OPC size distributions from TRACE-P for representative cases of biomass burning and pollution. At 3 km over Hong Kong we encountered a typical aged biomass aerosol plume (Figure 4a) with a moderately high concentration. At 350°C the mode shifts to smaller diameters but preserves a clear monomodal shape with ~85% or so of the total original number remaining and 40% remaining at sizes above 0.1 μm. A similar plot for an urban sample (Figure 4d) shows a greater shift upon heating and ~60% of the total number remaining but only 20% remaining with sizes larger than 0.1 μm.

[26] The changes indicated in the overall DMA distributions are confirmed when TDMA heated scans are done on sizes selected near 0.1 μm. In the biomass example, ~93% become smaller upon heating to 350°C with only ~3% remaining near the original size. The latter may be externally mixed or associated with very little volatile material (Figure 4b). A similar example for urban sources (Figure 4e) shows that ~5% of the total number remains in the selected size range after heating. However, both the biomass and urban distributions reveal that ~80% of the submicrometer volume is lost upon heating to 350°C (Figures 4c and 4f). The TDMA biomass example exhibits a shift in size that preserves a nearly monomodal shape compared to the urban case that shows a broader distribution after heating also evident in the full DMA distributions. This size shift with a large change in mass for a small change in number indicates an aerosol that is primarily internally mixed. In all cases, most aerosols present in the accumulation mode are internally mixed with a refractory component. We have observed similar differences in biomass versus urban measurements of refractory distributions that were measured over the Indian Ocean and off the coast of South America. These observations all indicate larger sizes with narrower refractory (presumed to be soot/BC) distributions in biomass plumes compared to broader distributions in urban plumes. The greater range of refractory sizes for the urban cases may reflect the multiplicity of diverse combustion sources compared to biomass sources.

3.4. Separating Out Refractory Dust and BC

[27] In Figure 5 we generalize our OES distributions for the entire ACE-Asia data set at times when dust concentrations exceeded ~40 μg m^{-3} in order to explore characteristics of the dust mode and the refractory soot (BC) mode. Coarse particle concentrations below this value can be common in polluted air even when wind-driven dust is not present. These data represent 10 min averages for all refractory OES distributions. Figure 5a reveals several distinctive features. Sizes below ~0.6 μm show variability over ~2 orders of magnitude. Between 0.6 and 2.0 μm most distributions have similar slopes and vary within ~1 order of magnitude. The curves diverge more at larger sizes and vary by ~2 orders of magnitude near 10 μm. Data from

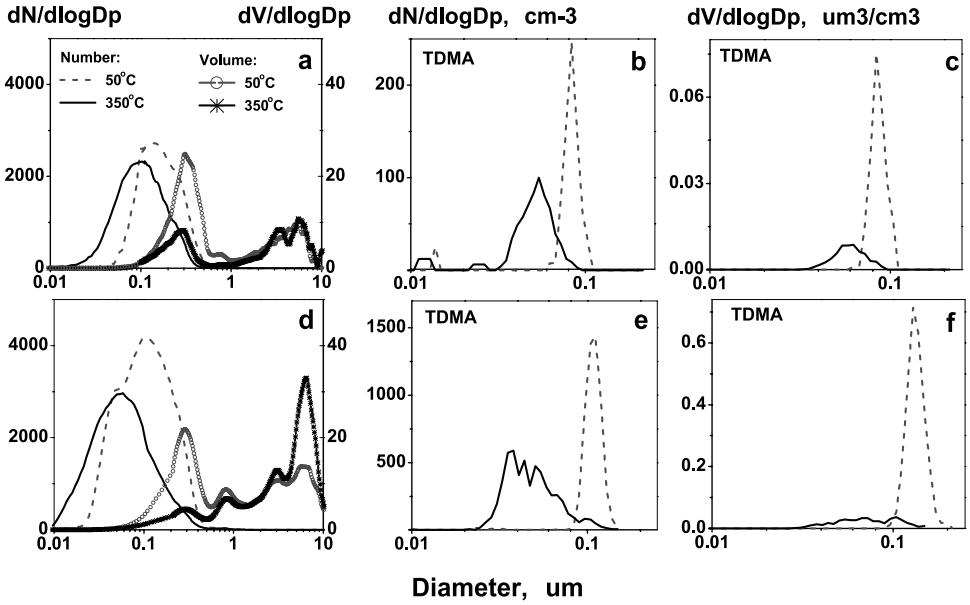

Figure 4. (a, d) Examples of unheated and heated DMA-OPC distributions showing number and volume volatility which ignore statistically uncertain data for $D_{OE} > 3$ μm. Corresponding TDMA (b, e) number and (c, f) volume which reveal internal mixtures of volatile species with refractory components for (top) biomass and (bottom) urban emissions. Urban refractory components (soot) are generally smaller and spread over a larger size range than biomass aerosol but in both cases most of the number are conserved, while volume is reduced to ~15% of original values indicating an internal mixed aerosol.

three legs flown on flight 13 at 5500 m (blue), 700 m (red), and 250 m (green) are highlighted as these three sequential legs range from the highest to relatively low-dust cases and moderate to lowest soot cases and span the range of aerosol mixes observed during ACE-Asia.

[28] The relative invariance of the slope of the dust mode below 2 μm suggests that the shape of the typical dust distribution might be approximated such that the refractory dust and soot modes could be separately resolved. It was found that consistent results were obtained by normalizing refractory distributions at diameters between ~0.65 and 1.2 μm. Because 0.75 μm D_{OE} is about the same as the 1 μm aerodynamic size cut (assuming a density of 2 μg m^{-3}) used for various size segregating impactors on ACE-Asia, including the nephelometer [*Anderson et al.*, 2003], we elected to use this diameter for normalization. The greater variability at the largest dust sizes is a result of the sensitivity of these sizes to production and removal processes. Sizes near 1 μm are resistant to removal processes and change less over time and distance from source [*Schutz*, 1980]. Variability in the refractory accumulation mode is driven largely by soot/BC, as demonstrated in section 3.6.

[29] After normalization, the variation in the refractory distribution (Figure 5b) is greatly reduced up to ~3 μm diameter while the soot mode retains a spread over ~2 orders of magnitude. The flight 13 legs at 250 and 700 m now fall on top of each other at the larger sizes, while the leg at 5500 m bounds the lower range of dust cases included here and the lowest of the soot cases. Although the soot mode for this case is small, both direct measurements and optical properties indicate that soot absorption is present (see section 3.6). As a result of these observations we have also indicated our so-called "reference" dust distribution for the high-dust case decreases rapidly at D_{OE} below 0.5 μm. The refractory volume distribution below 0.75 μm ($V_{ref<75}$), after subtracting our reference dust distribution, represents the refractory soot and includes the absorbing BC component. This approach assumes that all the refractory soot is confined to sizes below 0.75 μm, but we demonstrate that this assumption is not always true in section 3.7.

[30] Figure 5c shows the normalized refractory number distributions for the 250 m leg along with our reference dust distribution (RefDust) on flight 13. This was one of the largest dust concentrations during ACE-Asia and with highest concentrations of large particles. We therefore assume that it represents distributions characteristic of strong events with least aging. The shape of the reference dust mode was fit with three lognormal modes, and the remaining soot mode was fit with a single lognormal. Three dust modes have also been identified by other investigators, and two examples are included in Table 1. In order to properly extract the soot mode, our dust modes were established by recognizing (1) the stability of the dust mode near 1 μm and (2) our need to obtain a careful fit to the lower tail of that mode (dust 1). Actual fitting was carried out using the area distribution to resolve a peak in the larger dust mode usually between 5 and 9 μm. We also recognized that our coarse particle mode (dust 3) was poorly constrained at diameters above ~12 μm so we used a recently determined dust 3 fit [*Alfaro et al.*, 1998] for Saharan dust that appeared consistent with our data. The dust 1 fit was optimized by constraining the mode diameter to be larger than our normalization diameter of 0.75 μm and the standard deviation to be larger than 1.3 while minimizing differences

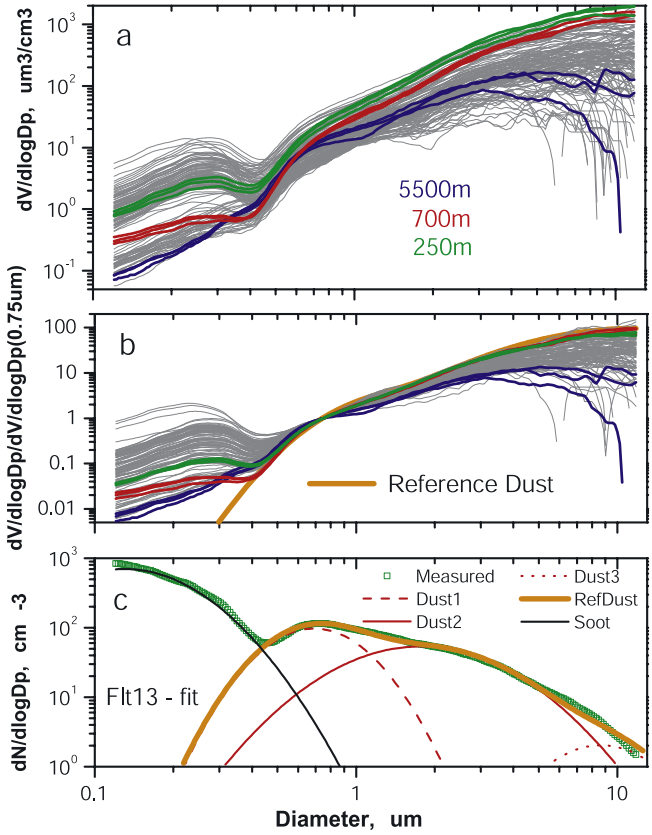

Figure 5. Size distributions (OES) of the refractory aerosol component (300°C) averaged over 10 min for all of ACE-Asia and with flight 13 highlighted for flight legs at 5500 m (blue), 700 m (red), and 250 m (green). (a) Variability in absolute concentrations. (b) Concentrations normalized at 0.75 μm (~1 μm aerodynamic) to characterize coarse dust component. Note stability of dust mode between 0.75 and 2 μm evident in tight envelope of low variation. (c) Normalized refractory number distributions for flight 13 at 250 m including lognormal fits to various modes used to separate out soot and dust variability (see text and Table 1). Highest dust concentrations in ACE-Asia are clearly evident at the 250 m leg (green) where the refractory accumulation mode (soot) volume has intermediate values.

between model and measured area and volume and number distributions in the vicinity of the fit. The mode diameter and standard deviation of the second dust mode, dust 2, was then allowed to vary until it also minimized differences between measured and model distributions for our normalized high-dust cases.

[31] Once these lognormal modes were established, we applied an optimizing technique to adjust the mode amplitudes to best fit our dust OES distributions. These three dust modes are compared to three mode fits recently published by *Alfaro et al.* [1998] and earlier frequently used fits described by *d'Almieda* [1987] in Table 1. Our dust distributions represent those measured on the order of 1000 km or so from source regions, and we would expect the larger third dust mode to be more variable closer to sources. The steep fall off in RefDust volume on this log-log plot below ~1 μm and the more gradual increase to a maximum near

Table 1. Lognormal Fit Parameters to the Refractory Number Distributions Shown in Figure 5c[a]

Lognormal Mode	Soot	Dust 1	Dust 2	Dust 3
This study				
MMD, μm	0.27	1.06	5.51	14.2
Standard deviation	1.59	1.46	1.85	1.5
d'Almieda [1987]				
MMD, μm		0.83	4.82	19.36
Standard deviation		2.10	1.90	1.60
Alfaro et al. [1998]				
MMD, μm		1.5	6.7	14.2
Standard deviation		1.7	1.6	1.5

[a] D_{pi} is the geometric mean or median diameter, and σ_i is the geometric standard deviation as defined by *Seinfeld and Pandis* [1998].

10 μm is also consistent with results from the Sahara [*Schutz*, 1980].

3.5. Refractory Aerosol and Absorption

[32] Apart from obtaining fits to OES distributions suitable for modeling the optical properties of the Asian dust distributions, our primary objective in fitting the smaller tail of the dust mode is to better resolve the size distributions of the absorbing soot/BC mode. To demonstrate this capability, we plot both the integral refractory volume distribution below 0.75 μm D_{OE} ($V_{ref<75}$) against the measured submicrometer

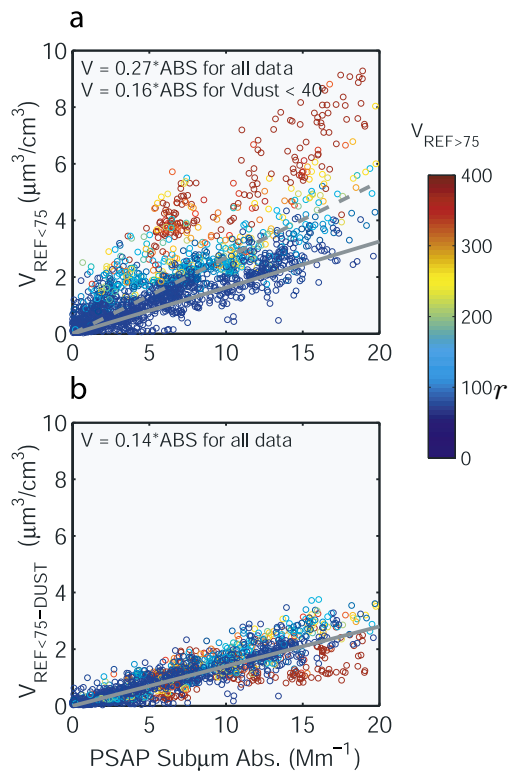

Figure 6. Plots showing effectiveness of our dust distribution at extracting dust tail from soot in refractory accumulation mode (fly ash cases removed). (a) Plot of $V_{ref<75}$ versus PSAP submicrometer absorption color coded by dust volume, $V_{ref>75}$. Dashed line is regression for all data, and solid line is for low dust with $V_{ref>75} < 40$ μm^3 cm^{-3}. (b) Same as Figure 6a for $V_{ref<75\text{-}Dust}$ after dust is subtracted, which clearly collapses data down to relation for soot-dominated data (blue).

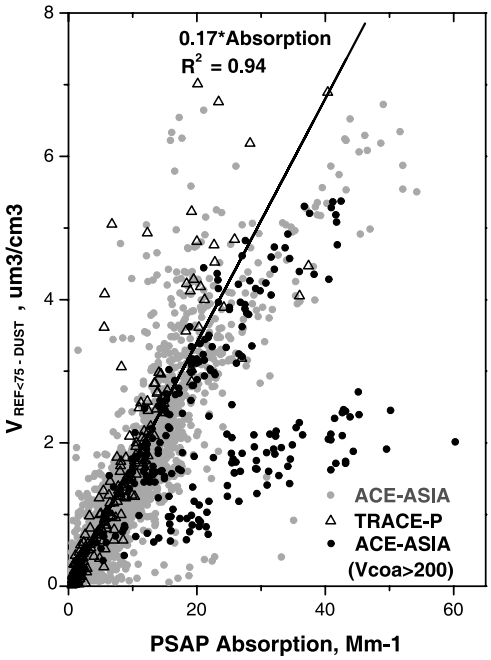

Figure 7. "Signature" plot of accumulation mode refractory soot volume with dust tail removed versus total aerosol light absorption. (a) TRACE-P (triangles) and ACE-Asia data. Note the strong linear relation for TRACE-P and most of ACE-Asia where absorption is dominated by refractory soot mode. Deviations above this relationship represent occasional addition of submicrometer nonabsorbing aerosol expected to be fly ash (e.g., SiO_2) in Yellow Sea rarely present on TRACE, and deviations to higher total absorption below line reflect coarse particle absorption from dust as evident in points highlighted as solid dots for coarse aerosol volumes >200 μm^3 cm^{-3} (see text).

PSAP absorption in Figure 6a. In Figure 6b we plot this volume with the dust component subtracted ($V_{ref<75\text{-}Dust}$). Figures 6a and 6b are color-coded by the total coarse dust volume. For clarity, ~5% of the ACE-Asia data (mostly some low-altitude legs over Yellow Sea) has been removed from both plots for cases of unusually high submicrometer fly ash with high submicrometer refractory volume and low absorption (see Figure 7 and discussion below).

[33] Figure 6a shows that for a given value of submicrometer PSAP absorption the values of $V_{ref<75}$ are highest when coarse dust concentrations are highest (red points). This reflects the increasing contribution of submicrometer dust, with low submicrometer absorption, to $V_{ref<75}$ as dust concentrations increase. The slope of the line (0.16) through the lower limit of data points for low-dust concentrations (below 40 μm^3 cm^{-3}, blue points) reveals the strong relationship between $V_{ref<75}$ and light absorption due to absorption by soot for low dust. If our reference dust distribution is representative of Asian dust and if our scheme for extracting the submicrometer dust volume from $V_{ref<75}$ is appropriate, then we expect a similar strong relationship between the submicrometer absorption and our submicrometer refractory volume when the submicrometer dust component is removed ($V_{ref<75\text{-}Dust}$). This is clearly evident in Figure 6b where these data collapse down from a slope of 0.27 to a similar slope of 0.14 when our reference dust is subtracted. Note that each data point is for refractory volumes measured over the last 30 s (~6 km) at 300°C during a 90 s temperature cycle and compared to average PSAP data over that period such that uncertainty in both measurements contribute to the scatter in the points. Even so, if our dust subtraction were too large, then $V_{ref<75\text{-}Dust}$ values would be consistently low and show up as data points well below other nondust (blue) cases. Conversely, if the dust subtraction were too little, these data would not have been collapsed as effectively. Hence our fit to the submicrometer refractory dust tail must be quite good. Exceptions are evident in the deep red data points when dust concentrations approach 400 μm^3 cm^{-3} (~1000 μg m^{-3}). At these dust concentrations the extracted soot volume fraction is well below 1% of the dust volume. Consequently, as long as the refractory soot volume exceeds 1% of the dust volume, this approach defines the dust shape well enough to allow us to reliably isolate the refractory soot distribution. At higher dust concentrations this approach can lead to an underestimate of residual soot.

[34] The strong relationship in Figure 6b also confirms the linear relation between $V_{ref<75\text{-}Dust}$ and the absorbing component. BC does not break down in air until heated above 700°C [*Smith and O'Dowd*, 1996]. Hence the refractory $V_{ref<75\text{-}Dust}$ must include the refractory light-absorbing BC that dominates the light absorption coefficient. Other likely components of the refractory aerosol other than dust include nonabsorbing (or relatively low absorbing) refractory organic carbon (OC) remaining at over 300°C and fly ash. Related studies in the Indian Ocean Experiment (INDOEX) suggest that about half of the refractory mass in this mode can be refractory OC stable at this temperature [*Mayol-Bracero et al.*, 2002], as discussed in section 3.9.

[35] Following the approach described for Figure 6, we again show our submicrometer extracted refractory soot volume, $V_{ref<75\text{-}Dust}$ (measured every 90 s), now plotted against the measured PSAP total absorption coefficient for both TRACE-P and ACE-Asia experiments (Figure 7). There are fewer data points for TRACE-P because measurements of absorption were cycled between total and submicrometer (aerodynamic), while two PSAP instruments provided continuous data for ACE-Asia. This cycling for TRACE-P also introduces some intrinsic scatter in TRACE-P absorption data because measurements are sequential and not coincident in time. Even so, $V_{ref<75\text{-}Dust}$ is closely related to total absorption in TRACE-P with an R^2 of 0.94.

[36] The ACE-Asia data in Figure 7 also show this strong relationship with a slope similar to TRACE-P, but there are some groups of data that lie above this slope and also below this slope. We note that the few high values for $V_{ref<75\text{-}Dust}$ evident in Figure 7 that fall above the primary linear relationship are not associated with elevated dust. These anomalous cases are generally from the Yellow Sea, and we believe that they reflect high concentrations of spherical submicrometer particles characteristic of low-absorbing coal fly ash. These were often found in large quantities during industrial coal feeding operations near Beijing during 2001 [*Shi et al.*, 2003], and most had diameters below 0.3 μm. This is also consistent with small silicate cenospheres generated by low-temperature coal combustion from old power plants that have been identified in this region (T. Cahill, personal communication, 2002; J. Anderson,

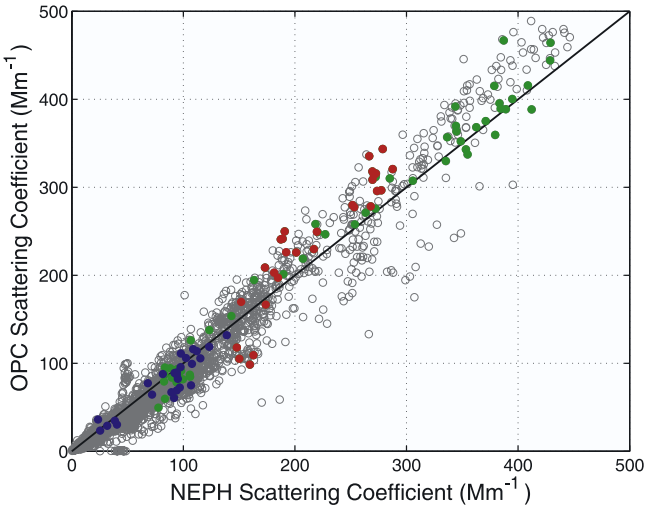

Figure 8. Plot of light scattering calculated from the OPC size distributions against measured scattering for scattering angles 7–170° as "seen" by nephelometer for all data (flight 13 highlighted). Data fall near 1:1 line when scattering is dominated by submicrometer aerosol, but for values dominated by dust the calculated values are ~10% larger than measured.

personal communication, 2002). Cases below the regression line reveal a higher absorption than cannot be accounted for by $V_{ref<75\text{-}Dust}$. This additional absorption is not related to BC but to dust, as evident for cases highlighted when coarse dust volumes exceeded ~200 μm^3 cm^{-3} (or ~500 μg m^{-3}, a moderate but arbitrary choice). Note that the TRACE-P data, where very little dust was encountered, have very few cases below the regression line. This plot is a useful way to identify most refractory dust, soot, fly ash through their "signatures" in their refractory sizes, and optical effects.

3.6. Refractory Size Distributions and Absorption: Dust Refractive Index

[37] We determine the best refractive index for the Asian dust by establishing consistency between measured and calculated scattering, absorption, and ϖ for both the total and submicrometer OPC size ranges. Because we must extract the dust size distribution from the total to get the soot components, we focus first on dust by analyzing observations during the heaviest dust case encountered during ACE-Asia flight 13 over the Yellow Sea. This allows us to examine the limiting behavior for dust absorption. The volatility data (Figure 2) reveal a low soot component for the leg near 5.5 km but higher soot concentrations near the surface. Consequently, we use these cases to help illustrate, explore, and constrain the real and complex refractive indices for the absorbing dust and soot components.

[38] The heated and unheated size distributions during this period (e.g., Figure 2) indicate that most particle volume is refractory dust with some volatile particles in the accumulation mode. We assume that dust is the dominant coarse particle absorber for highest dust concentrations in these cases. Therefore the complex refractive index for the observed dust size distribution that generates the observed absorption should be the maximum value for the dust. The presence of additional stronger absorbers (e.g., BC) would mean that the contributions from dust to measured coarse PSAP absorption could be even less. Our approach assumes that the influence of a small amount of absorption on OPC derived scattering is negligible. For the absorption considered here this was calculated to be <5%. The imaginary part of the refractive index of dust at 550 nm wavelength is initially assumed to lie between 0.0003 and 0.0052, while the real part was fixed at 1.53 [*Woodward*, 2001]. A percent or so variation about the real part is common in the literature, but this yields negligible changes in calculated scattering. Hence the OPC D_{OE} of the dust as measured are used directly for the Mie calculations. As mentioned earlier, the diameters of volume equivalent spheres are likely to be smaller than D_{OE} since irregularly shaped particles scatter more than equivalent spheres [*Kalashnikova and Sokolik*, 2002; *Koepke and Hess*, 1988; *Mishchenko et al.*, 1997]. However, at this point we are interested in measured and modeled optical properties so it is only the measured D_{OE} that concerns us.

[39] Comparison of values calculated over nephelometer measurement angles between 7° and 170° (Figure 8), and with flight 13 data highlighted as in Figure 5, to those measured on horizontal legs confirms that scattering calculated from OES distributions is reasonably consistent with the measured nephelometer scattering over a large range. This approach avoids the ambiguity in any error in the truncation correction for the nephelometer when particles sizes are very large [*Anderson et al.*, 1996]. The scattering angle of the OPC is only 35° to 145°, and hence our OES sizes also assume similar scattering between OES calibration spheres and ambient aerosol outside that angular range. Calculations suggest that this influence is expected to be small, but because side scatter is relatively enhanced for irregularly shaped particles, we expect a tendency to oversize them by the OPC. Calculated and observed scattering is similar for values below 150 Mm^{-1} where dust influence is small. As scattering increases because of dust, the calculated values trend ~10% higher than measured. This may be due to the effect just mentioned and/or a coarse aerosol calibration uncertainty for the OPC coarse sizes or transmission differences to the respective instruments for coarse aerosol.

[40] Our objective is to get a complex refractive index for our dust sizes consistent with data measured by the PSAP. However, in comparing PSAP data with OPC sizes we need to be aware of transmission losses for larger particles in the PSAP. We have measured this in the laboratory as a function of OPC effective optical size over a range of flow rates (not shown) for resuspended volcanic ash that had a "dust-like" size distribution. We found the PSAP at 1 L min^{-1} had a transmission of 50% at 12.5 μm D_{OE} and 80% at 7 μm D_{OE}. This leads to a small correction for absorption on ACE-Asia at highest dust loadings. The 4 L min^{-1} volumetric flow rate on TRACE-P requires larger size-dependent corrections, but the TRACE-P experiment encountered little dust so, with isolated exceptions, these corrections were negligible. Because neither the OPC nor the PSAP samples particles effectively above ~10–12 μm, our observations are limited to sizes below this.

[41] These considerations allow us to examine the coarse particle PSAP absorption in terms of the size distribution. To facilitate this, we define the volume absorption efficiency

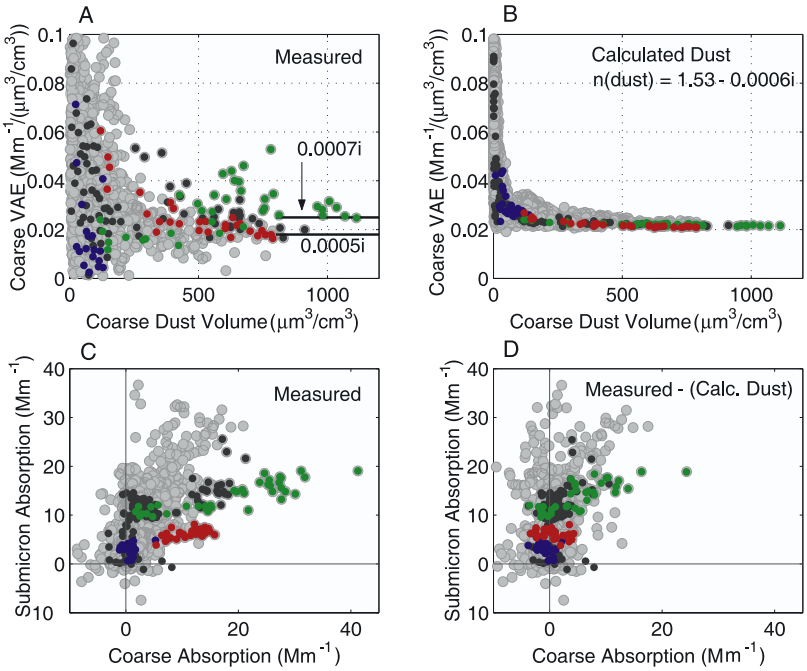

Figure 9. Asymptotic behavior for plot of coarse particle volume absorption efficiency (VAE) versus coarse particle V_{OE} with flight 13 flight legs highlighted. Asymptote constrains value of dust refractive indices between $k = 0.0007$ and 0.0005. (a) VAE as measured; (b) VAE calculated based for $k = 0.0006$ and impactor transmission that includes some accumulation mode soot in coarse mode; (c) PSAP submicrometer absorption versus coarse absorption (note net positive slope of data); (d) PSAP submicrometer absorption versus coarse absorption after subtracting model dust absorption (note more compact data cloud with many points corrected to near zero absorption but slope remains similar for remainder). (See text.)

(VAE) as the coarse particle absorption, as measured by the PSAP, per unit volume (V_{OE}) as measured by the OPC. Because of the sigmoidal size cut of the PSAP impactor the measured PSAP coarse absorption (total minus submicrometer) includes a tail that extends below 1 μm aerodynamic (~0.75 μm optical) that may include some soot. We also apply this sigmoidal size cut to the D_{OE} to determine the effective coarse V_{OE}. We argue that as coarse particle volume increases (high dust), the PSAP coarse particle absorption will be dominated by dust absorption. Hence, when VAE is plotted against coarse particle volume, it should asymptote to a value characteristic of the dust. It is this behavior that places strong constraints upon the maximum dust complex refractive index. A plot of this measured VAE versus coarse dust volume is shown in Figure 9a (the color codes from Figure 5 are preserved here). At lower dust V_{OE} the VAE is noisy and variable due to the coarse particle absorption being obtained from a small difference between total and submicrometer absorption. However, as coarse dust absorption increases, the noise is reduced, and these data are seen to asymptote to values near 0.022 Mm^{-1} μm^{-3} cm^3. On the basis of an assumed density for dust of 2.5 g cm^{-3} and a possible V_{OE} reduction up to 25% due to shape effects (see section 6), this value for VAE corresponds to a dust MAE of ~0.009 ± 0.002 m^2 g^{-1}. Mie calculations for the measured OES distributions and these asymptotic VAE values also constrain k to fall between ~0.0005 and 0.0007, as indicated. Similar calculations of the mass scattering efficiency (MSE) for the typical dust distributions yield a representative value of 0.31 m^2 g^{-1}.

[42] In Figure 9b we show the calculated values for VAE versus coarse dust volume for $k = 0.0006$ and how it asymptotes to the expected value. The higher VAE values for dust concentrations below 200 μm^3 cm^{-3} are primarily a consequence of the sigmoidal size cut of the PSAP impactor (0.75 μm D_{OE}) that allows some soot aerosol to be included in the coarse mode. This contribution has less effect as dust absorption increases. Moreover, for these particle sizes the difference between spherical and nonspherical absorption cross sections are calculated to be only ~2% [*Mishchenko et al.*, 1997] and imply that this refractive index applies equally well to the irregular dust aerosol.

3.7. Influence of BC Upon Dust Optical Properties

[43] Figure 9c shows a plot of submicrometer PSAP absorption versus coarse PSAP absorption (total less the submicrometer PSAP absorption). We first note that the cloud of all ACE-Asia data in light gray suggests a positive background slope. Because of the short 90 s sample time, there is considerable scatter present. Much of this is due to PSAP signal-to-noise ratio over this short sample time as evident by the physically meaningless negative values for both submicrometer and coarse absorption. Also note that we have stratified these data for low-dust cases only (below 20 or 50 μg m^{-3}) and found (not shown) that the slope for this subset of data shows coarse absorption to increase with submicrometer absorption. Figure 9c also includes the coarse absorption due to dust clearly evident in the highlighted data from flight 13. These observations imply that absorbing soot does exist in the coarse mode in the pollution

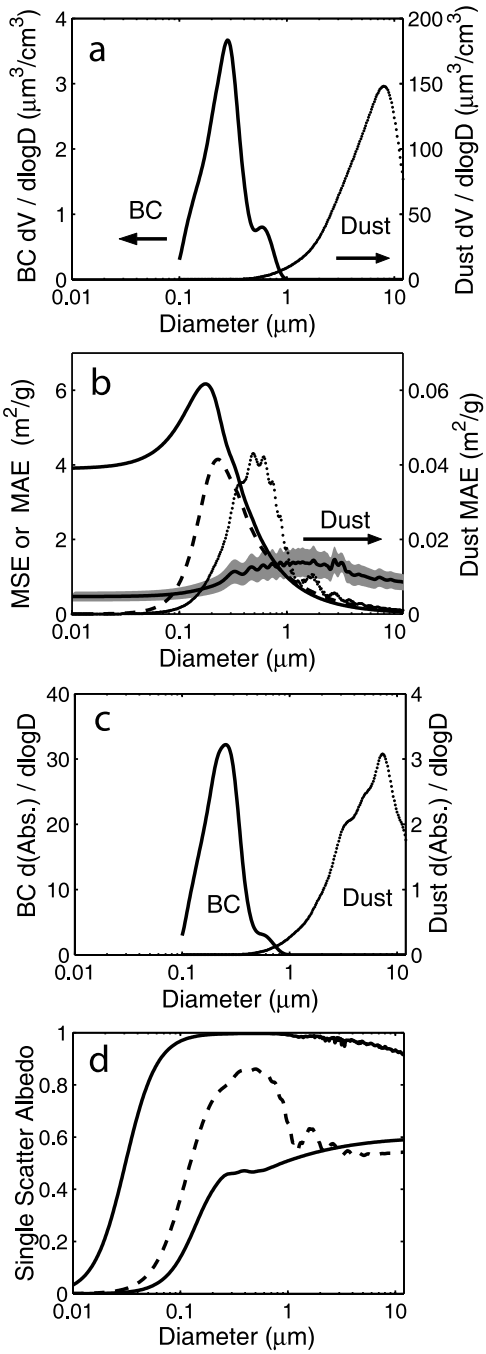

Figure 10. (a) Typical distributions representative of BC (assumed same as refractory soot-black) and dust (dots). (b) Calculated size-dependent MSE (dashed) and MAE (solid) properties modeled for BC and dust (dust MAE on right axis based on range of refractive indices discussed in text). (c) Absorption distributions representative of BC and dust. (d) Size-dependent ϖ for dust is near 1 for submicrometer distribution (top curve) and near 0.45 for pure BC distribution shown in Figure 10a (bottom curve) and near 0.8 for a mix of BC with nonabsorbing volatiles (dashed curve) similar to that of ACE-Asia aerosol.

aerosol independent of the presence of dust. The sigmoidal size cut for the impactor [*Wang and John*, 1988] leads to some BC/soot aerosol being removed by the impactor and not measured by the PSAP in the submicrometer mode. However, large soot aerosol has also been identified in some sources near Beijing [*Shi et al.*, 2003] and can be in larger sizes than we typically retrieve in our extracted soot distributions.

[44] Figure 9d is the same as Figure 9c only except that the modeled dust absorption using $k = 0.0006$ has been subtracted from PSAP coarse absorption. This clearly reduces absorption for most of the highlighted dust cases to within the cloud of variation for most of these data even for this fast 90 s average sampling rate. The cloud of gray circles has also narrowed. This change between Figures 9c and 9d reveals the degree to which coarse absorption was due to dust. Also note that the cluster of data (gray circles) in Figure 9c for submicrometer absorption between 20 and 30 Mm^{-1} have been separated into values that now have coarse absorption near zero and other values that show little change. The former are cases where coarse absorption was accounted for by dust, while the latter imply that considerable soot remains in the coarse mode. We note that individual soot carbon particle aggregates in the Beijing region with imaged diameters larger than 0.7 μm have been shown to comprise from a few percent to as much as 30% of the total [*Shi et al.*, 2003].

[45] However, Figure 9d shows a significant number of data points still to the right of the cloud of data even after correcting for dust absorption. This suggests that typically <15% but occasionally 30% or more of measured submicrometer absorption can show up in the coarse mode. We have examined these cases individually, and they are not the highest dust cases. This could indicate another dust type with a higher k value, but since highlighted green and red data are for two legs through the same plume, this seems unlikely. Many of these cases did occur in low-level pollution when some of the lowest ϖ values near 0.7 were observed. Even so, when we stratified for low-dust cases, there were very few examples of coarse absorption due to coarse soot exceeding $\sim$8 Mm^{-1}. Hence we do not believe these data arise from an underestimate in dust absorption due to larger dust not characterized by the OPC. Rather, we believe that they are due to larger absorbing aerosol either with or attached to the dust as seen by the PSAP (e.g., see Figure 2).

3.8. Refractory Size Distributions and Absorption: Soot

[46] We have shown that the accumulation mode is predominately internally mixed with a refractory soot component often dominated by absorbing BC. Refining the characteristic shape of the optically effective dust component allowed us to remove its contribution to submicrometer aerosol refractory volume and to better determine the refractory soot-only volume. These considerations and the strong relationship between volatility and soluble ions (S. G. Howell, personal correspondence, 2004) allow us to make assessments of how size-resolved scattering and absorption provide constraints on aerosol intensive properties such as effective real and complex refractive indices and the size-resolved MSE and MAE.

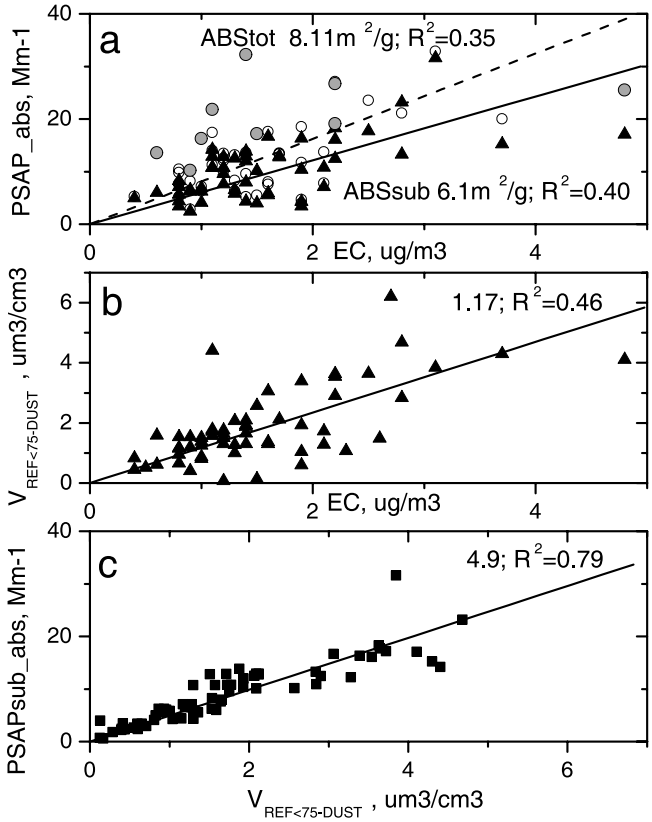

Figure 11. (a) Relationships between absorption of BC to EC over sample periods for EC of ~30 min. Slopes and correlations are indicated for total and submicrometer PSAP measurements. Solid circles indicate absorption influenced by elevated dust concentration above ~500 μg m^{-3}. The MAE values from the slope of the regression from 6.1 m^2 g^{-1} (submicrometer) to 8.1 m^2 g^{-1} (total aerosol). (b) $V_{ref<75\text{-}Dust}$ versus EC reveals a similar correlation coefficient as relationship in Figure 11a. (c) Correlation between PSAP absorption and $V_{ref<75\text{-}Dust}$ are much higher with R^2 of 0.75 and slope value is VAE. The combination of Figures 11a, 11b, and 11c demonstrates that the EC measurement has the largest uncertainty associated with it.

[47] Mie calculations of the size-dependent optical properties of soot and elevated dust aerosol are based on our measured D_{OE} shown in Figure 10a. Here we employ the dust refractive index 1.53−0.0006*i*, as determined above, and a BC refractive index of 1.95−0.66*i* representative of BC in diesel soot [*Bergstrom*, 1972; *Fuller et al.*, 1999]. The imaginary part of the complex refractive index of soot mixtures (BC plus refractory OC plus volatiles, etc.) will depend upon the fraction of absorbing BC that they contain. Figure 10b shows that the calculated MAE for "pure" BC approaches a peak value near 6 m^2 g^{-1} near 0.2 μm diameter and a constant value near 4 m^2 g^{-1} for much smaller sizes. Calculated MAE values continually drop with an inverse dependence on size above ~0.3 μm because of incident light being absorbed in the surface layer of the BC particles while the shielded mass toward the center does not contribute to absorption. Thus the large hollow "balls" shown in Figure 2 contribute a lot to BC absorption measurements but have low BC mass. If we assume that BC has the same size distribution as the submicrometer refractory aerosol sizes (Figure 10a), then the integral effective MAE is calculated at ~4.7 m^2 g^{-1}. However, BC aerosol is often made up of smaller BC primary sizes near 0.1 μm such that the MAE of the cluster can be close to the MAE of the primary particle (FMK). As a result, the integral MAE for pure BC with this refractive index may lie between 4.7 and 6 m^2 g^{-1}.

[48] These and other more complex effects (see FMK) need to be considered. However, if we simply apply the refractive indices already mentioned to the size distributions shown in Figure 10a for soot and dust, we obtain the size-distributed absorption for the soot and dust components shown in Figure 10c. The magnitudes of the absorption from BC and dust vary with their relative contributions to the aerosol, but the peak in the BC absorption contribution is near diameters of 0.3 μm while that of dust is at diameters over an order of magnitude larger. Figure 10d illustrates the calculated size-dependent values of ϖ for the typical dust, pure BC, and mixtures of soot and soluble species. We used a volume-weighted mixture of BC and volatiles, etc. (81% volatile, 6% BC and 13% refractory OC, see below), in the submicrometer accumulation mode as suggested by our volatility and refractory OC fractions observed in INDOEX [*Mayol-Bracero et al.*, 2002]. This model of homogenous mixing is not realistic (FMK) but provides a sense of possible optical properties. The submicrometer values of ϖ for the dust component are essentially 1 but drop to ~0.9 for D_{OE} near 10 μm. Values of ϖ calculated for the mixed aerosol sizes between 0.15 and 0.75 μm are seen to range from ~0.7 to 0.86 depending upon variations in the effective volume (mass) mean diameters for this mode (commonly between 0.2 and 0.5 μm). These are much higher than indicated values for pure BC that are near 0.44 at diameters near 0.2 μm. Actual values will probably differ due to various aspects of the mixing state not considered here (see FMK).

3.9. Refractory Soot, BC and EC Relationships, and MAE Values

[49] The mass absorption efficiency (MAE) for the BC aerosol can be obtained from measured PSAP absorption and the estimated mass of absorbing carbon. Measurements of elemental carbon mass (EC) based on CO_2 evolved from heated samples can also be related to aerosol light absorption and the refractory size distribution containing BC. A variety of EC techniques are used which differ in their approach and the manner in which EC is operationally defined [*Lim et al.*, 2003]. ACE-Asia employed the approach developed by Sunset Labs [*Huebert et al.*, 2003]. Leg average samples for EC of ~30 min duration were required in order to obtain a reasonable signal-to-noise ratio. These leg average regressions between BC absorption, refractory volume, and EC are shown for the ACE-Asia data in Figure 11a for data below 2 km where higher concentrations generally give EC data their best signal to noise. Three very anomalous values for EC were removed because they were not expressed in either BC absorption or OPC refractory volumes.

[50] Figure 11a shows that EC is related to both submicrometer and total measured PSAP absorption with an R^2 of

~0.40. Uncertainty arises both through some measurements being near detection limits and as a result of the operational definition of EC that includes the correction for charring of OC to BC. The two indicated regression slopes for submicrometer and total absorption yield an MAE of 6.1 and 8.1 $m^2\ g^{-1}$. As we mentioned in the discussion of Figure 9, on average, ~10% of the total soot absorption was expressed in the PSAP coarse size range. Hence the EC measurement on the total aerosol sampled is best compared to the total PSAP absorption for most samples. However, the larger MAE values for the PSAP total data also include additional absorption due to dust. Solid circles in Figure 11a highlight data for elevated dust with coarse volumes >200 $\mu m^3\ cm^{-3}$ and reveal the role of dust in generating outliers for this relationship. With these considerations in mind, the MAE for BC inferred from the limited EC measurements and their uncertainty indicate a representative value of $\sim 7 \pm 2\ m^2\ g^{-1}$.

[51] As demonstrated in Figures 7 and 8, the absorbing BC is a dominant part of the submicrometer refractory volume with dust removed. The plot of $V_{ref<75\text{-}Dust}$ against EC in Figure 11b has an R^2 value of ~0.46. If we assume that $V_{ref<75\text{-}Dust}$ is pure BC with an estimated density of ~1.9 g cm^{-3} (FMK), then the estimated mass of this $V_{ref<75\text{-}Dust}$ exceeds corresponding EC values by a factor of ~2.2. If we assume the measured EC is the absorbing BC, then it suggests ~45% of our $V_{ref<75\text{-}Dust}$ is absorbing BC on average. This is in line with thermo-optic analysis for other Asian aerosol (INDOEX [*Mayol-Bracero et al.*, 2002]) that found that the CO_2 evolved at temperatures above 300°C includes refractory OC that contributes ~60 ± 10% of the CO_2 evolved from the absorbing BC mass. Little other refractory mass was reported by Mayol-Bracero et al. As mentioned earlier, nonabsorbing and refractory submicrometer fly ash could confound this interpretation. However, such cases are only ~5% of the data set, as evident in the few points significantly above the line in Figure 7.

[52] Figure 11c shows $V_{ref<75\text{-}Dust}$ data averaged over flight legs corresponding to the EC measurements. It demonstrates that $V_{ref<75\text{-}Dust}$ is far better correlated with submicrometer BC absorption (R^2 of ~0.79) than with EC. This shows that EC measurement uncertainty is a source of the lower correlations in Figures 11a and 11b and encourages our use of refractory volume to assess MAE for the soot/BC combinations. However, the mean relation to EC data evident in Figure 11b remains a useful reference. In order to estimate the MAE of the absorbing BC based on our OPC $V_{ref<75\text{-}Dust}$ data we need to account for proper conversion of our V_{OE} to refractory aerosol mass and the absorbing BC component. Adjustments for the OPC sizing should be applied for highly absorbing aerosol [*Pinnik et al.*, 2000], and we have previously noted oversizing of ~8% by the OPC for pure BC aerosol with diameters below ~0.4 μm [*Clarke*, 1991]. Because our $V_{ref<75\text{-}Dust}$ is expected to be less than half BC by volume, we expect a smaller effect of say 3% such that actual submicrometer refractory volumes are estimated to be ~90% of measured OPC V_{OE}. However, the sigmoid cut of the PSAP impactor also removes ~10% of the BC as estimated from our OPC $V_{ref<75\text{-}Dust}$ (Figure 9 discussions). Consequently, these effects should be compensating when we compare $V_{ref<75\text{-}Dust}$ with mean submicrometer PSAP values, as in Figure 11c.

[53] Furthermore, the actual OC mass during ACE-Asia is related to the measured CO_2 evolved from OC by a multiplier of ~1.4 based on separate analysis of OC functional groups for ACE-Asia [*Russell*, 2003]. We assume here that the refractory OC in ACE-Asia and TRACE-P experiments has the same proportion of CO_2 evolved relative to BC (i.e., 60 ± 10%) as in INDOEX. However, the multiplier used on INDOEX was assumed to be 1.7 when correcting to OC mass [*Mayol-Bracero et al.*, 2002]. Application of the 1.4 multiplier to the CO_2 evolved from the refractory OC implies that the actual refractory OC mass is ~85% of the BC mass. Hence, for an OC density of 1 g cm^{-3} and a BC density near 1.9 g cm^{-3} (FMK) we expect 40% of our volume, $V_{ref<75\text{-}Dust}$, will be BC and 60% will be OC. Hence, if 40% of $V_{ref<75\text{-}Dust}$ is BC with a density of 1.9 g cm^{-3}, then we can convert the indicated slope in Figure 11c to an MAE for BC by dividing by 0.4 and dividing by density. This yields an MAE of 6.7 $m^2\ g^{-1}$. We recognize that the OC volume fraction is poorly constrained. However, the high correlation in Figure 7 implies that this fraction does not vary widely between ACE-Asia and TRACE-P, and we expect the latter BC sources to be similar to INDOEX values. Consequently, if we consider the refractory OC fraction (as CO_2) for INDOEX to range from 50% to 70%, then we get an uncertainty in MAE of $6.7 \pm 0.7\ m^2\ g^{-1}$. Alternately, if this assessment were made assuming the 1.7 multiplier mentioned above for conversion to OC mass instead of 1.4, then the MAE would be 7.6 ± 0.8 $m^2\ g^{-1}$. These values are also remarkably consistent with the range of values based on EC estimated from Figure 11a.

[54] It is important to keep in mind that these MAE values are obtained from the measured PSAP absorption for the internally mixed submicrometer aerosol. This includes possible enhancements to pure BC absorption arising from the state of mixing (FMK). Higher MAE values for BC would also be obtained if BC were a smaller fraction of the refractory component (i.e., BC plus high-temperature OC) than used above. However, a smaller fraction would be inconsistent with most INDOEX data (O. L. Mayol-Bracero, personal correspondence, 2003) and the relation indicated in Figure 11b. This implies that the range of MAE values above should be representative of these data sets.

4. Influence of Dust on BC Optical Properties

[55] Earlier we indicated a possible perturbation of dust optical properties arising from the coagulation of BC with the dust mode. However, the presence of dust surface area can also be expected to influence the accumulation of volatiles including sulfuric acid and OC vapors [*Tang et al.*, 2004]. In the absence of enhanced Asian dust these species commonly reside in the accumulation mode and on other coarse pollution aerosol (e.g., Figure 3, bottom). Because these species are associated with the combustion in the source regions, we might expect them to be found in characteristic ratios with BC for a given region and time. Also, because the BC component is formed at high temperatures in the combustion process, these volatile components

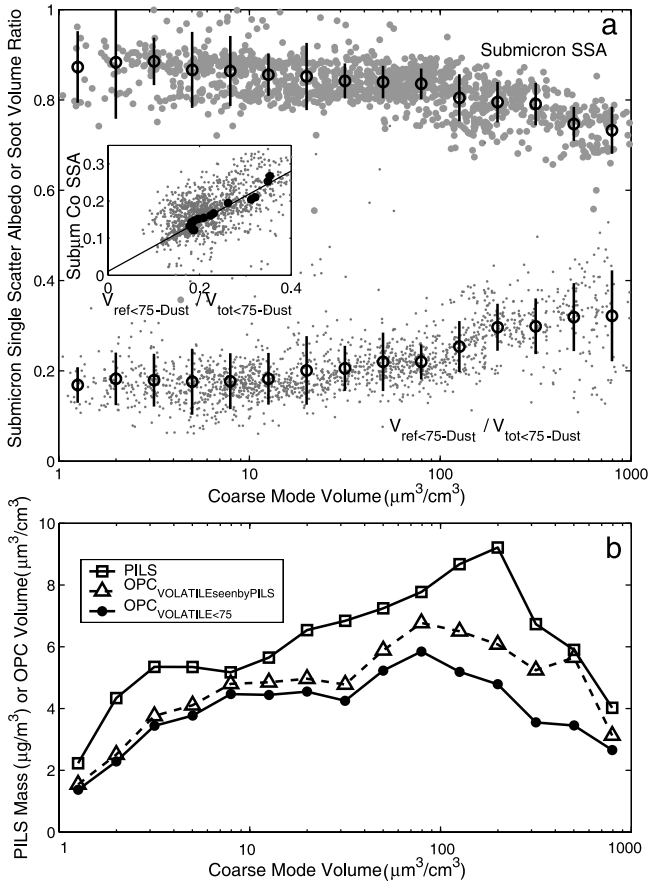

Figure 12. (a) Plots of the refractory soot fraction [$V_{ref<75\text{-}Dust}/V_{tot<75\text{-}Dust}$] of the accumulation mode volume and the ϖ for the submicrometer mode as a function of coarse dust volume obtained every 90 s on all horizontal legs below 2 km during ACE-Asia. As the fraction of refractory soot increases (less volatiles), less submicrometer scattering is contributed by volatiles due to their uptake onto coarse aerosol. This results in the lower values for submicrometer ϖ. Bin-averaged values over equal log intervals of coarse volume are highlighted for both parameters. Coalbedo (1-ϖ) is plotted against $V_{ref<75\text{-}Dust}/V_{tot<75\text{-}Dust}$ in the insert. Large solid points are the regional average values based on the bin averages shown and have a slope of 0.68 and an R^2 of 0.94. These indicate that the mix of BC to volatiles in the submicrometer mode and its regional optical properties are strongly influenced by the dust. (b) Corresponding bin-averaged values of PILS combined sulfate, nitrate, and ammonium mass. The total volatile volume estimated to be "seen" by PILS is below 1.2 μm and the total volume is below 0.75 μm D_{OE} as a function of the coarse dust volume. Peak values occur at coarse volume concentrations characteristic of urban pollution and drop at higher concentrations of dust consistent with loss to the dust.

will be added to the BC after its emission. Condensates like combustion-derived OC may promptly deposit to aerosol surface, while others, like sulfates, would take longer because photochemical processes are required. If BC is generated and emitted into dusty air with elevated surface area, then significant fractions of these components may accumulate on the dust instead of becoming associated with soot/BC in the accumulation mode.

[56] Figure 12a shows the ratio of the refractory volume, $V_{ref<75\text{-}Dust}$, to total accumulation mode aerosol, $V_{tot<75\text{-}Dust}$ (dust removed), obtained from our OPC volatility data. These data are from all ACE-Asia horizontal legs below 2 km altitude. They are shown for over three decades of coarse particle volume along with average values binned over equal log intervals of coarse particle volume. These average values are presumed to reflect regional characteristics for the ACE-Asia domain during April 2001. Coarse particle volume includes contributions from typical background dust, industrial dusts, or fugitive emissions as well as significant Asian dust transport events moving through the region. These coarse volume values can be put in context when compared to PM_{10} data for urban Beijing in 2001. A weekly average in March was ~360 μg m^{-3} (150 μm^3 cm^{-3}) and in April was 200 μg m^{-3} (80 μm^3 cm^{-3}), while in the low-dust and low-heating-fuel period of September it was ~130 μg m^{-3} (50 μm^3 cm^{-3}) [*Shi et al.*, 2003]. In view of these values we assume that our Figure 12 data collected in April 2001 will have coarse volumes of ~60 μm^3 cm^{-3} associated with strong urban pollution signatures even when desert dust is not present. We also assume that values much larger than this indicate enhanced incursions of Asian dust into the region.

[57] There is a very gradual decrease in the submicrometer refractory volume ratio as the coarse volume falls below ~50 μm^3 cm^{-3}. However, when coarse volumes exceed this value, the submicrometer refractory volume fraction of the accumulation mode [$V_{ref<75\text{-}Dust}/V_{tot<75\text{-}Dust}$] clearly increases as the dust volume increases. Because most $V_{ref<75\text{-}Dust}$ is emitted from combustion sources, it should not vary because of the presence of dust. Hence we argue that this ratio changes due to the increased uptake of condensate unto the coarse dust surface. This leads to an increase in the fraction of refractory soot/BC left in the accumulation mode.

[58] This is confirmed in Figure 12b, where we plot volatile volume below 0.75 μm as measured by the OPC versus the coarse mode volume. Also shown is the volatile volume for D_{OE} smaller than 1.2 μm expected to be measured by the PILS. The third plot shows the combined mass for sulfate, nitrate, and ammonium ions measured from PILS. These all display a similar behavior. Peak values are evident for coarse concentrations near 80 μm^3 cm^{-3}, as would be expected for values representative of the polluted urban environment. As dust concentrations increase to over 500 μm^3 cm^{-3} (1250 μg m^{-3}), these volatile species and soluble ions drop to about half of their peak values consistent with the increase of $V_{ref<75\text{-}Dust}$. Also note the consistency in the drop for both measured PILS mass and the volume estimated for the PILS from the OPC data. When coarse volumes drop well below 50 μm^3 cm^{-3}, the volatile volume and the PILS ionic mass (Figure 12b) also decreases steadily while the [$V_{ref<75\text{-}Dust}/V_{tot<75\text{-}Dust}$] (Figure 12a) changes slowly. This can be understood in view of the range of locations and altitudes represented in this data set. Scattering and absorption (and associated refractory submicrometer aerosol) decrease with altitude, and the variability is large (Figure 1). Below 2 km this variability is often due to dilution of near-surface air by

mixing with clean air aloft. Clean air can often have very low concentrations of both refractory and volatile aerosol. Hence mixing will generally dilute near-surface pollution concentrations but have a smaller effect on the ratio [$V_{ref<75\text{-}Dust}/V_{tot<75\text{-}Dust}$]. Clear air aloft also tends to have a greater fraction of more volatile nonabsorbing aerosol that is consistent with the gradual decrease in refractory volume and increase in ϖ (Figure 12a) as coarse volume decreases.

[59] We demonstrated earlier (Figure 2) that BC in the accumulation mode usually contributes only a small fraction of the total accumulation mode volume even though it dominates the absorption. Hence the scattering properties of the accumulation mode are generally dominated by the volatile/soluble component often accumulated on the soot aerosol. Consequently, when the refractory fraction of the accumulation mode increases, we might expect the value of submicrometer ϖ to decrease. This is shown to be the case in Figure 12, where the lowest values of submicrometer ϖ are associated with the highest dust cases and trend to lower values with an increasing refractory volume fraction present in the accumulation mode. Although the dust tail present in the submicrometer mode contributes refractory aerosol with ϖ near 1 (see Figure 10d), the reduction in scattering due to loss of volatile species has the greater effect. The result is lower values for submicrometer ϖ measured in the high-dust cases even though ϖ for the total aerosol increases due to dust. The strong relationship between these two ratios is evident when we plot the coalbedo (1-ϖ) against the refractory volume fraction. The correlation for the individual points (90 s data) has an R^2 of only 0.4, and most of the points are concentrated at the lower range of values. However, these rapid measurements include uncertainties arising from the short sample times for PSAP data mentioned earlier in conjunction with Figure 9 and due to the sequential nature of the OPC heated and unheated scans. Also, far more cases occur for low and intermediate values of both measurements than for high. However, the regional average values (solid black circles), obtained by binning over the dust concentration intervals shown in Figure 12a, better reveal their relationship as a result of increasing dust concentrations. This relationship has a slope of 0.68 and an R^2 of 0.94 and indicates a strong regional influence of dust upon both the typical optical and microphysical properties of the pollution mode aerosol. We return to this and related issues in section 6.

5. Comparison of Measured BC to Model Values

[60] One of the objectives of TRACE-P and ACE-Asia was to obtain information on aerosol and gas phase properties over scales and times that could be used to challenge chemical transport models (CTM). Several modeling groups were involved with these experiments, but the University of Iowa group [*Carmichael et al.*, 2003] employed their CTM in support of both experiments and included the modeling of BC. In Figure 13 we present some initial comparisons of model results for BC_{model}, measured PSAP light absorption and $V_{ref<75\text{-}Dust}$ for both campaigns. Because each point is a measurement of only 90 s, it captures details of atmospheric variability not resolved on the scales of the model or the meteorological data that the CTM is based on. Hence a pointwise comparison is not our objective, but rather we are interested in broad indications of consistency or inconsistency with regional model data.

[61] Emissions of CO are a major combustion indicator carried in many models so we have used the ratio of measured CO to model CO in order to identify cases where measured CO is higher than model values by 20% or more (Figure 13a). In Figure 13b we show PSAP absorption versus BC_{model} for TRACE-P where biomass plumes were common and dust absorption was negligible. It is stratified here by the ratio of $CO_{measured}$ to CO_{model} for values above and below a value of 1.2. This provides a gauge of model performance for combustion derived CO where ratios larger than 1.2 indicate model underestimates for CO. The slopes shown on Figure 13a are the MAE_{model} for the model when evaluated based on the ratio of measured PSAP absorption to BC_{model}. The regression for cases when the CO_{model} is within 20% of measured values has a slope of 7.7 $m^2\ g^{-1}$, while for the cases when CO_{model} underestimates observed values the regression is $\sim$17 $m^2\ g^{-1}$. The former value is consistent with expected MAE values determined above, while the latter value is high and indicative of the BC_{model} being too low.

[62] Figure 13c shows a similar plot for ACE-Asia. However, biomass sources were a much smaller contributor to BC emissions in this region [*Ma et al.*, 2004; *Uno et al.*, 2003]. Here these data clearly suggest two branches. We have selected two constraints for these data to emphasize conditions where CO sources in the CTM inventory CFORS [*Streets et al.*, 2003; *Uno et al.*, 2003] were dominated by model combustion fuel sources (CFORS fuel CO >20 ppbv) and when they were dominated by biomass (CFORS biomass CO > 10 ppbv). These two dominant source types fall into the two separate branches. The biomass sources dominate the lower branch with a MAE_{model} of 7.2 $m^2\ g^{-1}$ based on an average for the constrained data and very similar to the TRACE-P value in Figure 13b. The upper branch indicates a typical MAE_{model} value near 32 $m^2\ g^{-1}$ and clearly higher by about a factor of 3 or more than can be justified.

[63] Figure 13d is an analysis similar to Figure 13c but demonstrates that our $V_{ref<75\text{-}Dust}$ versus BC_{model} reveals clearly the same features. In Figure 13e we return to our signature plot (Figure 7) of $V_{ref<75\text{-}Dust}$ versus PSAP absorption. Here the ACE-Asia data are shown with the same two constrained and highlighted data sets. Figure 13e confirms that highlighted CFORS biomass and CFORS fuel-dominated cases fall along the same slope. This slope is the VAE (proportional to MAE) for absorbing BC and implies differences of <10% in MAE for the two fuel types. This similarity demonstrates that both sources of the BC aerosol in the model have similar observed optical properties so that soot microphysics or optics cannot be a reason for these differences. Hence these observations indicate that current estimates of emissions [*Streets et al.*, 2003] used in CFORS for biomass BC appear to be consistent with our MAE for TRACE-P and ACE-Asia but that combustion fuel BC in the region north of 25°N may be a factor of 3 or so too low.

6. Discussion and Conclusion

[64] Thermal analysis of the size distributions of Asian aerosol provides insight into its physiochemical properties.

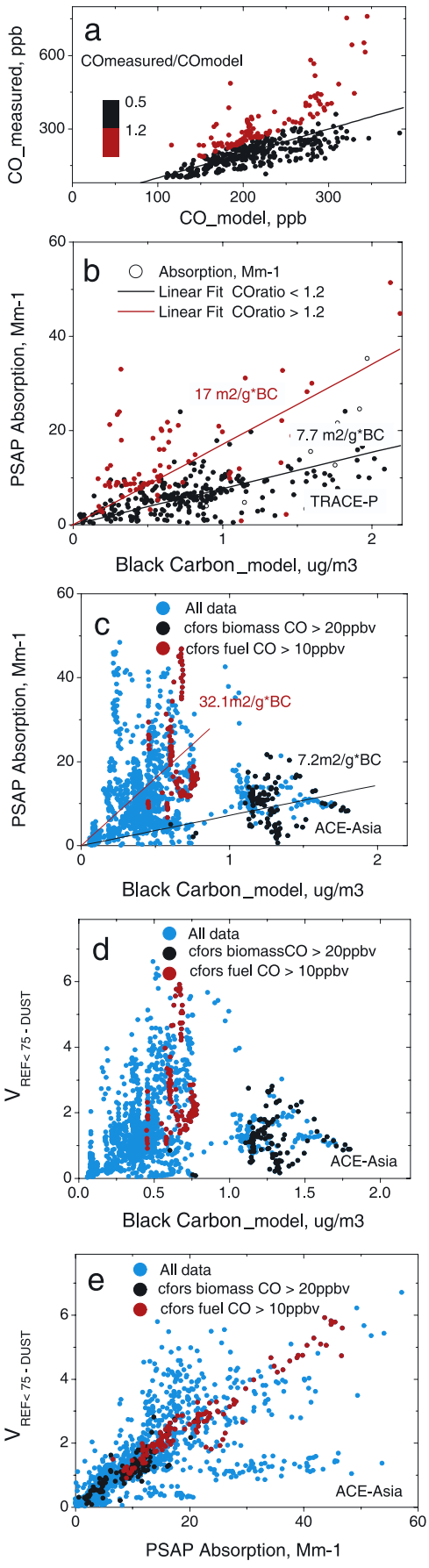

This approach demonstrates that BC and associated high-temperature emissions establish most of the aerosol number concentration by providing sites upon which other species (e.g., sulfate, nitrate, water) condense and/or heterogeneously react. These soluble species and organic components were mixed with soot in over two thirds of the aerosol and constituted most of the submicrometer volatile volume. TDMA data indicate that the refractory soot fraction is generally 10–25% of the total volume for sizes near 0.1 μm and typically 15–30% when averaged over the accumulation mode (Figure 12), but only about one third to one half (5–15%) of this is expected to be BC.

[65] Optically effective dust sizes were measured out to ~10 μm. Examination of coarse particle absorption per unit volume of dust as dust volume increases resulted in asymptotic values that constrain the complex refractive index for dust. These values were consistent with the measured absorption and scattering coefficients and imply a refractive index for Asian dust of $n = 1.53 - 0.0006i$ ($\pm 0.0001i$) when used for optically effective sizes. Unlike BC, the MAE for typical dust OES distributions has a maximum of ~0.009 $m^2\ g^{-1}$ near 2 μm and an MSE near 0.31 $m^2\ g^{-1}$. These optical properties results in ϖ values for the dust distribution that vary from ~1 for submicrometer sizes up to ~0.93 at 10 μm diameter, consistent with the effective coarse particle ϖ values observed near 0.97 [*Anderson et al.*, 2003] for dust-dominated cases. Optical properties were often well described by the presence of an accumulation mode with ϖ near 0.84 and a dust aerosol with ϖ near 0.97. Variations in relative contributions from both types account for significant variation in total ϖ observed. The statistically larger values for ϖ seen for Asian aerosol north of 25°N (TRACE-P) and those seen during ACE-Asia are explained by the greater prevalence of dust in the aerosol.

[66] However, in cases of pollution in the presence of high-dust concentrations, we observe larger refractory soot fractions in the accumulation mode and correspondingly lower submicrometer ϖ values than for the case of pollution with low dust. Dust should increase submicrometer ϖ because ϖ is near 1 for submicrometer dust (Figure 10d). Hence this decrease must be due to the relative increase in

Figure 13. Comparison of CTM model results for BC with results for CFORS BC emissions for TRACE-P and ACE-Asia. (a) Ratio of measured to models CO with values 20% higher or more than model highlighted to identify model underestimates. (b) Plot of PSAP absorption versus BC_{model} for TRACE-P data color stratified by ratio of measured to model CO concentrations. Average MAE values for both groupings are indicated as lines. (c) PSAP absorption versus BC_{model} for ACE-Asia showing a branched relationship. High model biomass and high model fossil fuel CO values are shaded and show up on different branches. (d) $V_{ref<75\text{-}Dust}$ versus BC_{model} for same data as Figure 13c, confirming that submicrometer refractory $V_{ref<75\text{-}Dust}$ reveals the same behavior for these highlighted cases. (e) Plot of $V_{ref<75\text{-}Dust}$ versus PSAP absorption showing that both data groups have the same slope (i.e., same MAE values) and confirms that differences are not related to soot optical properties but to model performance. (See text for details.)

the BC fraction of the accumulation mode as a result of uptake of volatile species onto the dust. This average influence can be quantified by making an approximate straight-line fit in Figure 12 between the soot volume ratio at ~80 and ~500 μm^3 cm^{-3} to get a linear expression for this ratio as a function of the logarithm of coarse mode volume, D_v. When combined with the linear expression between this ratio and coalbedo from the insert, one gets the following expression for ϖ in terms of D_v:

$$\varpi = 0.84 - 0.102 \log(D_v/80), \quad (1)$$

where D_v is OES dust volume in μm^3 cm^{-3}.

[67] In order to express this in terms of a more familiar mass concentration we not only have to use a dust density of ~2.5 g cm^{-3} to convert volume to mass but also must correct D_{OE} to geometric diameter. The latter is not well constrained, but for the angular range of our OPC of 35° to 145° the greatest change in scattering intensity for irregular dust relative to spheres occurs around 100°–145° [*Kalashnikova and Sokolik*, 2002], but this is also where the phase function has minimum values. We estimate from their assessment that the change in integral OPC scattering intensity due to shape effects is <20%. This will increase D_{OE} by <10% and our optical volume by <25% over an equivalent mass of dust. This is probably an upper limit of the shape effect on our OPC measurements, and smaller effects are likely (O. V. Kalashnikova, personal correspondence, 2003). Hence the above expression can be employed as an approximation when applied to measured dust mass, D_m, by replacing the term $D_v/80$ by $D_m/160$ (i.e., 160 = 80 × 2.5/1.25), where D_m is in μg m^{-3}. As an example, our regional pollution aerosol has a typical submicrometer ϖ of ~0.84 in the absence of high dust (Figure 12). When it is emitted into a mean dust concentration of 1000 μg m^{-3} (~500 μm^3 cm^{-3} OES), equation (1) predicts the value of submicrometer ϖ to be reduced to 0.75 because of the transfer of volatiles to the dust.

[68] This change in submicrometer ϖ is a result of the transfer of volatile mass from the accumulation mode to the dust. A detailed optical model of this effect must take into account the complex interaction of BC with condensed species (see FMK) at a level beyond the scope of this paper. However, some insight can be gained through a simple examination of the dependency of ϖ on MAE_a and MSE_a defined here for the accumulation mode mass, m_a. We can write this as follows:

$$\begin{aligned} \varpi &= \sigma_{sp}\left[\sigma_{sp} + \sigma_{ap}\right]^{-1} = \left[1 + \sigma_{ap}/\sigma_{sp}\right]^{-1} \\ &= \left[1 + \left(\sigma_{ap}/m_a\right)\left(m_a/\sigma_{sp}\right)\right]^{-1} \\ \varpi &= \left[1 + MAE_a/MSE_a\right]^{-1}, \end{aligned} \quad (2)$$

where σ_{sp} and σ_{ap} are the particle scattering and absorption coefficients, respectively, for the mixed accumulation mode.

[69] We assume here an internal mixture of soot/BC with volatiles and that the absorption is not significantly affected by this loss of volatiles. Hence the MAE_a for the accumulation mode mixture will change primarily in response to the loss of volatile mass from the accumulation mode to the dust. Our data in Figure 12 indicate that about half the volatile volume (~40% of the total volume) is lost to the dust when concentrations rise from ~80 μm^3 cm^{-3} characteristic of urban pollution to 800 μm^3 cm^{-3} in high-dust events. At the same time the refractory fraction increases from 20 to 30% of the total (Figure 12a). Ignoring density differences, this loss of 40% volatile volume implies that the MAE_a will increase by about a factor of 1.6. This loss will also reduce the remaining accumulation mode to 0.6 of its original volume or ~85% of its original diameter. This size change will decrease the effective MSE_a by ~15% or so for this aerosol (see Figure 10b). Consequently, the net effect of this high dust on equation (2) will be to change the ratio of MAE_a to MSE_a by a factor of about 1.6/0.85 = 1.9.

[70] Our observed regional average submicrometer ϖ in pollution with a coarse volume of 80 μm^3 cm^{-3} is 0.84 (Figure 12a). Equation (2) indicates that this corresponds to a ratio of MAE_a to MSE_a of 0.19 in the unperturbed pollution aerosol. When this value is multiplied by the factor 1.9, the new value for ϖ under high dust, as predicted by equation (2), is ~0.74 and in good agreement with Figure 12a for a coarse volume of 800 μm^3 cm^{-3}. Hence this simple approach demonstrates that the transfer of volatile material to the coarse dust mode is predictably linked to a corresponding change in submicrometer ϖ. We plan a more detailed investigation of this effect in a future paper.

[71] The amount of volatiles that can be expected to accumulate on the dust will depend upon the dust surface area, how long it is available for these species to interact with the dust, the dust surface chemistry, the chemistry of the accumulating species, the concentrations of the accumulating species and environmental process and conditions, etc. Even so, our data (Figures 12a and 12b) reveal that ~50% of the volatiles normally in the accumulation mode when no dust is present get transferred to the dust when high-dust concentrations mix with pollution in this region. Model calculations [*Tang et al.*, 2004] for similar dust concentrations indicate that ~30% of the sulfate and 80% of the nitrate can end up on the dust surface. Keeping in mind that our volatile components can include these species as well as some volatile OC, our observations are consistent with their model and tend to confirm the magnitude of their model results.

[72] This effect will result in accumulation of this scattering mass onto larger dust sizes with low effective MSE instead of onto the optically effective accumulation mode. As a result, the contribution to scattering extinction by these emissions (e.g., sulfate) will decrease significantly for mass transferred from sizes at 0.3 μm to sizes at 3.0 μm (see Figure 10b). Hence column optical depths or radiative forcing estimated from regional sulfur emissions can be in error as a result of their uptake onto the dust. Submicrometer ϖ will also be lowered compared to what might be expected if the pollution and dust modes were separately modeled with no interaction. Consequently, the optical properties of a mixture of dust and pollution aerosol will be different if they mix before or after most volatiles have been adsorbed. This means that the physical, chemical, and optical properties of pollution and dust aerosol that mix near sources are not additive for each source but must be modeled interactively. It also means that regional emissions of species such as sulfate cannot simply be scaled to a net radiative forcing without considering the aerosol environment into which they are emitted.

[73] Comparison of PSAP light absorption with measurements indicated that measured MAE values for EC lie in the range of $\sim 7 \pm 2$ m^2 g^{-1} (Figure 11a). However, the correlation coefficient with EC was $R^2 = 0.4$, so considerable scatter in these data is present. Thermally resolved submicrometer refractory volume was more highly correlated with submicrometer PSAP absorption ($R^2 = 0.79$), indicating that this refractory volume distribution contains the absorbing BC (Figure 11c). This refractory volume is known to also include OC remaining at 300°C [*Mayol-Bracero et al.*, 2002] where the latter can equal about half of the refractory mass (about 1/3 the refractory volume). MAE values based on these data were shown to lie in the range of 6–8.4 m^2 g^{-1}, consistent with the EC analysis. The comparison of EC and the refractory soot volume was also consistent with the INDOEX estimate of BC being about one half of the refractory submicrometer mass. These MAE values are also similar to data for BC measured on aircraft in INDOEX reported as 6.6–8.1 m^2 g^{-1} [*Mayol-Bracero et al.*, 2002] and to the MAE values inferred from the model data discussed for TRACE-P and ACE-Asia.

[74] BC in the accumulation mode tended to have a volume mean D_{OE} near 0.3 ± 0.2 μm. Mie calculations using the OPC refractory volume distributions and a refractive index of $1.95 - 0.66i$ were shown to yield a size-weighted submicrometer MAE of ~ 4.7 m^2 g^{-1} for the pure BC component when treated as BC spheres over the refractory size ranges. This is considerably lower than the values obtained above even though our assumed value of $k = 0.66$ is relatively high and mean values higher than this are not easy to justify. We believe that these differences probably arise due to enhancement effects arising from the internal mixture of BC with OC, sulfate, and other species. If large BC aerosol are aggregates of primary aerosol with sizes of 0.1–0.2 μm diameter, then larger BC clusters would have properties more like the primary sizes. This would yield MAE values closer to the peak value of 5 to 6 m^2 g^{-1} in Figure 10b. If the BC were usually on the surface of the accumulation mode aerosol, then an additional enhancement of 15% might raise average values to 6 to 7 m^2 g^{-1}, as per FMK.

[75] Additional enhancements from some BC being encapsulated in OC and volatile aerosol at the 10–20% BC volume fraction level could also increase these values for certain sizes. Such enhancements in absorption due to prescribed mixtures of BC and OC for sizes similar to our soot distributions have been recently demonstrated to approach a factor of 2 in the laboratory [*Saathoff et al.*, 2002]. Even so, if we allow for the probability of some BC with lower refractive indices than assumed here, the evidence for some BC present at larger sizes, a variable range of BC morphology, a variable state of mixing, etc., then an average values of a factor of 2 enhancement for Asian BC appears unlikely. Consequently, our above MAE values suggest a moderate enhancement of perhaps 50% over MAE values expected for pure BC but consistent with the most likely values estimated by FMK. These MAE values are lower than values of 11 ± 5 m^2 g^{-1} reported by *Mader et al.* [2002] but within their wide uncertainty range.

[76] A comparison of our BC absorption, refractory volume, and CTM model output for the chemical weather forecasting (CFORS) regional emissions indicates that emissions of BC [*Streets et al.*, 2003] encountered during TRACE and for dominant biomass sources during ACE-Asia regions are consistent with our measurements. However, some combustion fuel sources appear underpredicted by the model by about a factor of 3. This is similar to underprediction of CO also seen in the model for similar sources [*Streets et al.*, 2003; *Tang et al.*, 2004]. Other model results that employ the same emission inventory have found regional differences in measured and model BC that have been attributed to measurement differences [*Uno et al.*, 2003]. However, the model underestimates of BC indicated here can be expected to contribute significantly to these regional differences.

[77] BC is a primary emission upon which many other components condense to create an internal mixture. Hence BC accounts for ~85% of the observed accumulation mode number. As a result, the nature of the combustion process and how BC emissions and the number of BC particles are generated has implications for both direct and indirect forcing. Moreover, these results demonstrated that details of BC microphysical properties and its optical effects must be considered in conjunction with condensates associated with it as well as the full aerosol size distribution into which these emissions are mixed.

[78] **Acknowledgments.** This data collection and analysis was only possible through the combined support provided for TRACE-P (NASA NCC-1-416) and ACE-Asia grant support (NSF ATM00-02070). We are particularly grateful to the chief scientists D. Jacob, J. Crawford, and B. Huebert and support crews of the NASA P-3B and NCAR C-130. Special appreciation is extended to Program Managers, Vickie Connors (NASA) and Anne-Marie Schmoltner (NSF), for encouraging and supporting the intercomparison flights between the two programs that facilitated combining these data sets. Funding for UW participation was supported by NSF ATM-0002198 and ATM-0138250 and by NOAA (JISAO agreement NA37RJ0198). B.J.H.'s work was supported by NSF grant ATM00-02698 and amendments thereto. This research is a contribution to the International Global Atmospheric Chemistry core project of the International Geosphere-Biosphere Program. This is SOEST contribution 6355.

References

Alfaro, S. C., A. Gaudichet, L. Gomes, and M. Maillé (1998), Mineral aerosol production by wind erosion: Aerosol particle sizes and binding energies, *Geophys. Res. Lett.*, *25*(7), 991–994.

Anderson, T. L., et al. (1996), Performance characteristics of a high-sensitivity, three-wavelength, total scatter/backscatter nephelometer, *J. Atmos. Oceanic Technol.*, *13*(5), 967–986.

Anderson, T. L., S. J. Masonis, D. S. Covert, N. C. Ahlquist, S. G. Howell, A. D. Clarke, and C. S. McNaughton (2003), Variability of aerosol optical properties derived from in situ aircraft measurements during ACE-Asia, *J. Geophys. Res.*, *108*(D23), 8647, doi:10.1029/2002JD003247.

Bergstrom, R. W. (1972), Predictions of the spectral absorption and extinction coefficients of an urban air pollution model, *Atmos. Environ.*, *6*, 247–258.

Bond, T. C., T. L. Anderson, and D. Campbell (1999), Calibration and intercomparison of filter-based measurements of visible light absorption by aerosols, *Aerosol Sci. Technol.*, *30*, 582–600.

Carmichael, G. R., et al. (2003), Regional-scale chemical transport modeling in support of the analysis of observations obtained during the TRACE-P experiment, *J. Geophys. Res.*, *108*(D21), 8823, doi:10.1029/2002JD003117.

Clarke, A. D. (1991), A thermo-optic technique for in-situ analysis of size-resolved aerosol physicochemistry, *Atmos. Environ., Part A*, *25*(3/4), 635–644.

Clarke, A. D., and R. J. Charlson (1985), Radiative properties of the background aerosol—Absorption component of extinction, *Science*, *229*(4710), 263–265.

Clarke, A. D., T. Uehara, and J. N. Porter (1997), Atmospheric nuclei and related aerosol fields over the Atlantic: Clean subsiding air and continental pollution during ASTEX, *J. Geophys. Res.*, *102*, 25,281–25,292.

Clarke, A. D., J. L. Varner, F. Eisele, R. L. Mauldin, D. Tanner, and M. Litchy (1998), Particle production in the remote marine atmosphere:

Cloud outflow and subsidence during ACE 1, *J. Geophys. Res.*, *103*, 16,397–16,409.

Clarke, A. D., W. G. Collins, P. J. Rasch, V. N. Kapustin, K. Moore, S. Howell, and H. E. Fuelberg (2001), Dust and pollution transport on global scales: Aerosol measurements and model predictions, *J. Geophys. Res.*, *106*, 32,555–32,569.

d'Almieda, G. A. (1987), On the variability of desert radiative characteristics, *J. Geophys. Res.*, *92*, 3017–3026.

Fuller, K. A., W. C. Malm, and S. M. Kreidenweis (1999), Effects of mixing on extinction by carbonaceous particles, *J. Geophys. Res.*, *104*, 15,941–15,954.

Huebert, B. J., T. Bates, P. B. Russell, G. Shi, Y. J. Kim, K. Kawamura, G. Carmichael, and T. Nakajima (2003), An overview of ACE-Asia: Strategies for quantifying the relationships between Asian aerosols and their climatic impacts, *J. Geophys. Res.*, *108*(D23), 8633, doi:10.1029/2003JD003550.

Huebert, B., et al. (2004), PELTI: Measuring the passing efficiency of an airborne low turbulence inlet, *Aerosol Sci. Technol.*, in press.

Jacob, D. J., J. H. Crawford, M. M. Kleb, V. S. Connors, R. J. Bendura, J. L. Raper, G. W. Sachse, J. C. Gille, L. Emmons, and C. L. Heald (2003), Transport and Chemical Evolution over the Pacific (TRACE-P) aircraft mission: Design, execution, and first results, *J. Geophys. Res.*, *108*(D20), 9000, doi:10.1029/2002JD003276.

Kalashnikova, O. V., and I. N. Sokolik (2002), Importance of shapes and compositions of wind-blown dust particles for remote sensing at solar wavelengths, *Geophys. Res. Lett.*, *29*(10), 1398, doi:10.1029/2002GL014947.

Kaufman, Y., D. Tanre, O. Dubovik, A. Karniele, and L. Remer (2001), Absorption of sunlight by dust as inferred by satellite measurements and ground based remote sensing, *Geophys. Res. Lett.*, *28*, 1479–1482.

Koepke, P., and M. Hess (1988), Scattering functions of tropospheric aerosols—The effects of nonspherical particles, *Appl. Opt.*, *27*(12), 2422–2430.

Li, J., M. Posfai, P. V. Hobbs, and P. R. Buseck (2003), Individual aerosol particles from biomass burning in southern Africa: 2. Compositions and aging of inorganic particles, *J. Geophys. Res.*, *108*(D13), 8484, doi:10.1029/2002JD002310.

Lim, H. J., B. J. Turpin, E. Edgerton, S. V. Hering, G. Allen, H. Maring, and P. Solomon (2003), Semicontinuous aerosol carbon measurements: Comparison of Atlanta Supersite measurements, *J. Geophys. Res.*, *108*(D7), 8419, doi:10.1029/2001JD001214.

Ma, Y., et al. (2004), Intercomparisons of airborne measurements of > aerosol ionic chemical composition during TRACE-P and ACE-Asia, *J. Geophys. Res.*, *109*, doi:10.1029/2003JD003673, in press.

Mader, B. T., R. C. Flagan, and J. H. Seinfeld (2002), Airborne measurements of atmospheric carbonaceous aerosols during ACE-Asia, *J. Geophys. Res.*, *107*(D23), 4704, doi:10.1029/2002JD002221.

Mayol-Bracero, O. L., R. Gabriel, M. O. Andreae, T. W. Kirchstetter, T. Novakov, J. Ogren, P. Sheridan, and D. G. Streets (2002), Carbonaceous aerosols over the Indian Ocean during the Indian Ocean Experiment (INDOEX): Chemical characterization, optical properties, and probable sources, *J. Geophys. Res.*, *107*(D19), 8030, doi:10.1029/2000JD000039.

Mishchenko, M. I., L. D. Travis, R. A. Kahn, and R. L. West (1997), Modeling phase functions for dustlike tropospheric aerosol using shape mixture of randomly oriented polydisperse spheroids, *J. Geophys. Res.*, *102*, 16,831–16,847.

Moore, K., II, et al. (2004), A comparison of similar aerosol measurements made on the NASA P3-B, DC-8, and NSF C-130 Aircraft during TRACE-P and ACE-Asia, *J. Geophys. Res.*, *109*, doi:10.1029/2003JD003543, in press.

Orsini, D. A., Y. L. Ma, A. Sullivan, B. Sierau, K. Baumann, and R. J. Weber (2003), Refinements to the particle-into-liquid sampler (PILS) for ground and airborne measurements of water soluble aerosol composition, *Atmos. Environ.*, *37*(9–10), 1243–1259.

Pinnik, R. G., J. D. Pendelton, and G. Videen (2000), Response characteristics of particle measurement systems active scattering spectrometer probes, *Aerosol Sci. Technol.*, *33*, 334–352.

Russell, L. M. (2003), Aerosol organic-mass-to-organic-carbon ratio measurements, *Environ. Sci. Technol.*, *37*(13), 2982–2987.

Saathoff, H., C. Linke, O. Möhler, K. H. Naumann, M. Schnaiter, W. Schöck, R. Wagner, and U. Schurath (2002), Influence of coatings on structure and optics of soot aerosol, paper presented at IGAC Conference 2002, Crete, Greece. (available at http://imk-aida.fzk.de/abstract/)

Schutz, L. (1980), Long range transport of desert dust with special emphasis on the Sahara, in Aerosols: Anthropogenic and Natural Sources and Transport, edited by T. Kniep and P. Lioy, *Ann. N. Y. Acad. Sci.*, *338*, 515–532.

Seinfeld, J. H., and S. Pandis (1998), *Atmospheric Chemistry and Physics*, 429 pp., John Wiley, Hoboken, N. J.

Shi, Z., L. Shao, T. P. Jones, A. G. Whittaker, S. Lu, K. A. Berube, T. He, and R. J. Richards (2003), Characterization of airborne individual particles collected in an urban area, a satellite city and clean air area in Beijing, 2001, *Atmos. Environ.*, *37*, 4097–4108.

Smith, M. H., and C. D. O'Dowd (1996), Observations of accumulation mode aerosol composition and soot carbon concentrations by means of a high-temperature volatility technique, *J. Geophys. Res.*, *101*, 19,583–19,591.

Sokolik, I. N., and O. B. Toon (1999), Incorporation of mineralogical composition into models of the radiative properties of mineral aerosol from UV to IR wavelengths, *J. Geophys. Res.*, *104*, 9423–9444.

Streets, D. G., et al. (2003), An inventory of gaseous and primary aerosol emissions in Asia in the year 2000, *J. Geophys. Res.*, *108*(D21), 8809, doi:10.1029/2002JD003093.

Tang, Y., et al. (2004), Three-dimensional simulations of inorganic aerosol distributions in east Asia during spring 2001, *J. Geophys. Res.*, *109*, doi:10.1029/2003JD004201, in press.

Uno, I., G. R. Carmichael, D. Streets, S. Satake, T. Takemura, J. H. Woo, M. Uematsu, and S. Ohta (2003), Analysis of surface black carbon distributions during ACE-Asia using a regional-scale aerosol model, *J. Geophys. Res.*, *108*(D23), 8636, doi:10.1029/2002JD003252.

Wang, H. C., and W. John (1988), Characteristics of the Berner impactor for sampling inorganic ions, *Aerosol Sci. Technol.*, *8*, 157–172.

Weber, R. J., et al. (2003), New particle formation in anthropogenic plumes advecting from Asia observed during TRACE-P, *J. Geophys. Res.*, *108*(D21), 8814, doi:10.1029/2002JD003112.

Weber, R. J., D. Orsini, Y. Daun, Y. N. Lee, P. J. Klotz, and F. Brechtel (2001), A particle-into-liquid collector for rapid measurement of aerosol bulk chemical composition, *Aerosol Sci. Technol.*, *35*, 718–727.

Woodward, S. (2001), Modeling the atmospheric life cycle and radiative impact of mineral dust in the Hadley Centre climate model, *J. Geophys. Res.*, *106*, 18,155–18,166.

J. Anderson and X. Hua, Environmental Fluid Dynamics Program, Department of Mechanical and Aerospace Engineering, Arizona State University, University Blvd., Tempe, AZ 85287, USA. (janderson@asu.edu)

T. Anderson, D. Covert, and S. Doherty, Department of Atmospheric Sciences, University of Washington, Seattle, WA 98195-1640, USA. (tadand@atmos.washington.edu; dcovert@u.washington.edu; sarahd@atmos.washington.edu)

G. Carmichael, Department of Chemical and Biochemical Engineering, University of Iowa, 424 IATL, Iowa City, IA 52242, USA. (gcarmich@icaen.uiowa.edu)

A. D. Clarke, S. Howell, B. Huebert, V. N. Kapustin, C. McNaughton, K. G. Moore II, and Y. Shinozuka, Department of Oceanography, 1000 Pope Road, University of Hawaii at Manoa, Honolulu, HI 96822, USA. (tclarke@soest.hawaii.edu; showell@soest.hawaii.edu; huebert@hawaii.edu; kapustin@soest.hawaii.edu; cameronm@soest.hawaii.edu; kmoore@soest.hawaii.edu; yohei@hawaii.edu)

R. Weber, School of the Earth and Atmospheric Sciences, Georgia Institute of Technology, 221 Boddy Dodd Way, Atlanta, GA 30332, USA. (rweber@eas.gatech.edu)